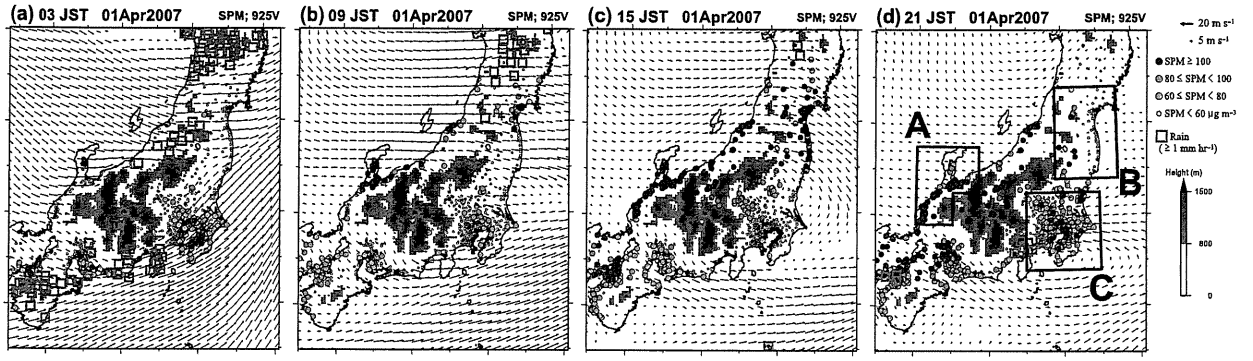

Fig. 2. SPM concentration (open circles: < 60 μg m^{-3}, green: 60–80, orange: 80–100, red: ≥ 100) at (a) 03 JST, (b) 09 JST, (c) 15 JST, and (d) 21 JST on 1 April 2007. Vectors show the 925-hPa winds from the GPV-MSM. Blue squares represent rainfall (> 1 mm hr^{-1}) at the Automated Meteorological Data Acquisition System (AMeDAS) observatories. Gray shading indicates the topography represented by GPV-MSM. Areas enclosed by thick solid lines in Fig. 2d (regions A, B, and C) are used to make Fig. 3.

sets). The cloud mask scheme and the discrimination procedure for cloud particle types have been fully documented by Hagihara et al. (2010) and Yoshida et al. (2010).

3. Results

Figure 2 shows the spatial distribution of SPM concentrations and horizontal wind at 925-hPa in central Japan. In the early morning of 1 April, strong southwesterly wind was observed ahead of a cold front off the southern coast of Japan through southern Kanto (Fig. 2a; see also Supplement 1). Although a rapid SPM increase was observed in the area, the high SPM sites (SPM ≥ 100 μg m^{-3}) were sporadically distributed and terminated at 08 JST. These high SPM values may have been caused by local emission of primary particles in Japan. At 09 JST on 1 April (Fig. 2b), the maximum SPM was 209 μg m^{-3} in Hokuriku. By 15 JST (Fig. 2c), high SPM sites advanced eastward from western Japan, Hokuriku, and southern Tohoku. At 21 JST (Fig. 2d), high SPM sites were widely observed in Kanto. The high SPM sites were first observed at 19 JST along eastern Kanto and subsequently moved to the inland area under easterly wind conditions. The easterly wind in Kanto was also confirmed by the GPV-MSM surface wind data (see Supplement 1) and the AMeDAS observed data (not shown).

Figure 3 shows areal SPM concentrations in regions A–C (Fig. 2d). In Region A (Fig. 3a), the median SPM (solid line) rapidly increased from 36 μg m^{-3} (08 JST) to 119 μg m^{-3} (10 JST) on 1 April. The median SPM peaked at 19 JST (175 μg m^{-3}) and gradually decreased afterwards. In Region B, the median SPM exceeded 100 μg m^{-3} at 13 JST and continued until 16 JST (Fig. 3b). However, the median SPM in Region C remained low (around 40 μg m^{-3}) during the daytime of 1 April and then increased to over 60 μg m^{-3} after 20 JST (Fig. 3c). From the time series of median SPM and meteorological conditions (i.e., rainfall and wind direction change) in Fig. 3, SPM increase over Kanto was considerably delayed compared with the increases in Hokuriku and Tohoku. According to three-dimensional wind measured by wind profilers and surface rainfall data, the arrival times of the cold front were 22 JST 31 March–01 JST 1 April (Region A), 01–04 JST 1 April (Region B), and 00–05 JST 1 April (Region C). The temporal differences between the passage of a cold front and the rapid SPM increase in those regions were approximately 10 hours (Region A and B) and 15–20 hours (Region C).

Figure 4 shows a time-height section of the dust extinction coefficient at Toyama and Tsukuba (see Fig. 1b). At Toyama, we can identify two dust layers in the daytime of 1 April (Fig. 4a), located above 3 km and below 2.5 km altitude. In particular, a severe dust layer (dust extinction coefficient > 0.3) was found near the ground with θ < 290 K. Meanwhile, two elevated dust layers are also shown at Tsukuba (Fig. 4b) at 3–4 km around the $\theta \approx$

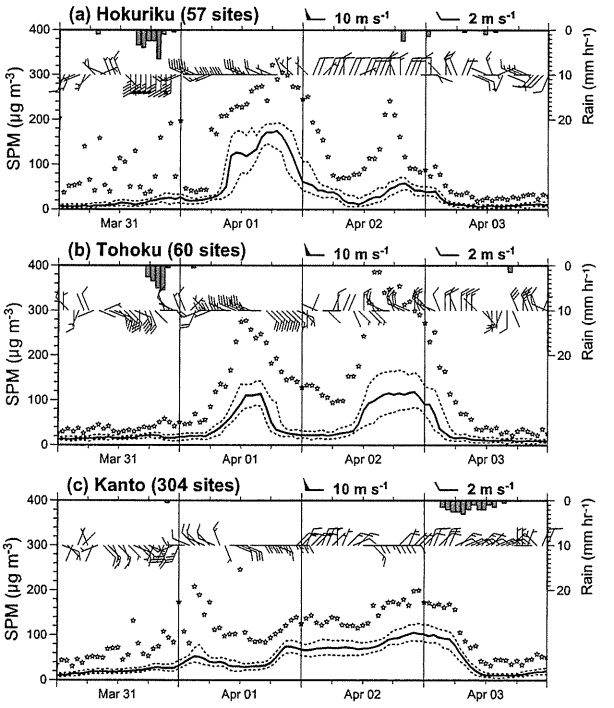

Fig. 3. Time series of areal statistics of SPM in (a) Hokuriku (Region A in Fig. 2d), (b) Tohoku (Region B), and (c) Kanto (Region C) during 31 March–3 April. Solid and dashed lines show the median and upper/lower quartiles of SPM, respectively. Star: maximum SPM. Rain intensity (downward bar) and surface wind (barb) at JMA observatories (Toyama, Sendai, and Tateno in regions A, B, and C, respectively) are also plotted.

310 K isentrope and around 1 km altitude at the $\theta \approx$ 296 K isentrope. The upper layer may have originated from the Taklimakan Desert (Yumimoto et al. 2008). After 18 JST on 1 April, another dust layer was observed at Tsukuba below 1 km altitude.

From Figs. 2–4 and Supplement 1, the regional-scale characteristics of the TAD-2007 episode are summarized as follows: (1) Most of the lower dust layer was contained in a cold air mass in Hokuriku, (2) dust arrival was delayed in Kanto compared to adjacent areas, and (3) high SPM in Kanto advanced westward from the east coast inland. These results suggest that the low-level dust layer passed around the central mountains and crossed southern Tohoku. After that, the dust-containing air may have been transported from the Pacific Ocean to inland Kanto in association with

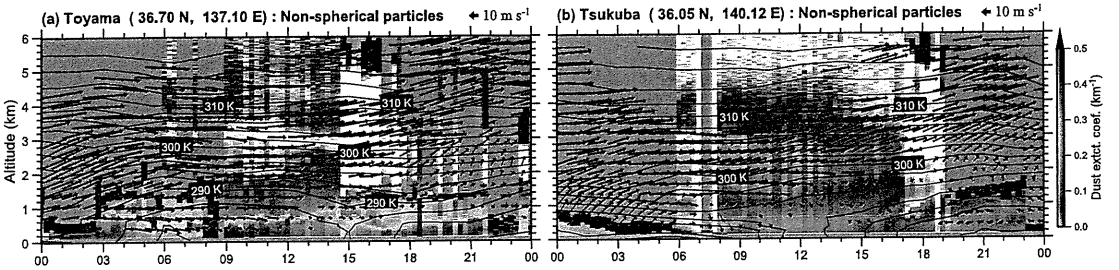

Fig. 4. Time-height section of a dust extinction coefficient (color; km^{-1}) at (a) Toyama and (b) Tsukuba on 1 April 2007. Black: cloud, gray: missing due to rain or above cloud layer. Three hourly θ (contour; 2 K interval) is obtained from the nearest grid of the lidar site in GPV-MSM. Horizontal wind (vector) is obtained from the nearest wind profiler observatories ((a) Takada, (b) Mito).

the advancing easterly wind (see Figs. 2d, 4b). In the next section, we discuss the above-mentioned processes along with other possibilities.

4. Discussion

We briefly examine the following three possible causes of the delayed dust transport in Kanto: (1) prevention of the downward transport of dust particles by a stably stratified layer (e.g., Tsunematsu et al. 2009), (2) wet deposition (e.g., Han et al. 2004), and (3) indirect transport around the central mountains (this study).

First, we examine the possibility of prevention of downward dust transport from an elevated dust layer in Kanto. Tsunematsu et al. (2009) noted that near-surface cold air inhibited a vertical mixing in the early morning of 1 April. The near surface cold air may have caused a delay in the development of planetary boundary layer (PBL). In other words, the delayed development of PBL may have contributed to the inhibition of downward dust transport from the upper layer to the surface and to the low SPM values in Kanto. As shown in Fig. 4a, most of the main dust layer in Toyama was below θ < 300 K throughout the dust period. Because the lower dust layer in Tsukuba was around the $\theta \approx 296$ K isentrope, it may have originated from the upper part of the main dust layer in Toyama. The θ profiles were almost neutral around noon, but the θ value was slightly smaller than that of the elevated dust layer (Fig. 4b). While previous studies suggested that the PBL development in Kanto brought dust down to the ground (Tsunematsu et al. 2009; Takahashi et al. 2010), the SPM change in Kanto was unclear during the day on 1 April (Fig. 3c). That is, the delayed development of PBL may have contributed to the low SPM in Kanto, but downward dust transport was not identified in Kanto during the daytime of 1 April.

Second, we discuss the influence of wet deposition. As shown in Fig. 1a, clouds covered wide regions around Japan. On one side of the Sea of Japan, the westerly wind was dominant in the dust layer (Figs. 2, 3). When high mountains block a dust containing air, dust particles may be scavenged by cloud condensation or rainfall along the mountain slope. However, precipitation radar and rain gauge observations did not detect rainfall over central Japan during the daytime of 1 April (not shown). Figure 5 shows a vertical profile of cloud reflectivity and cloud particle types based on the merged datasets. In the south of Japan, water clouds were dominant below 2 km altitude. In contrast, the clouds over mainland Japan were present above the mid-troposphere. A dense dust layer was located over the Sea of Japan around the $\theta \approx 290$ K isentropic surface. Over the Sea of Japan, high relative humidity layers were located above the mid-troposphere and the near surface level below the dense dust layer.

In the merged dataset, the main dust layer was categorized as "3-D ice" (randomly oriented ice crystals; for details see Yoshida et al. 2010). This categorization may have been caused by an extremely high dust concentration because the cloud mask in the merged datasets was determined by a large backscattering coefficient from CALIPSO observation. The Vertical Feature Mask (VFM) version 2 data developed by the CALIPSO team

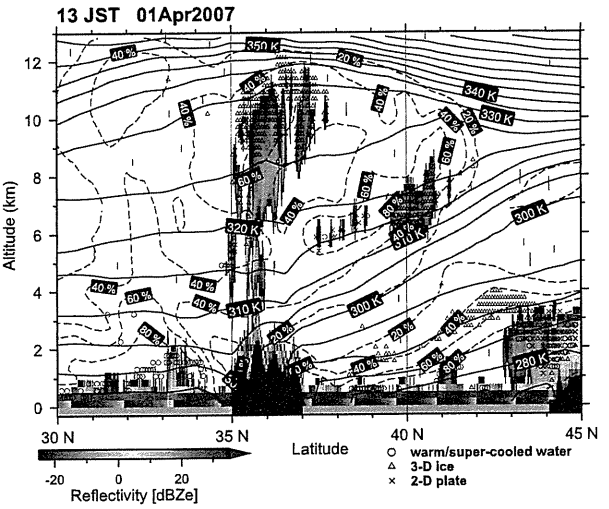

Fig. 5. Vertical profiles of radar reflectivity (color; dBZe), θ (solid; 5 K interval), RH (red dashed; 20% interval), and cloud particle types (symbol) across Japan (green line in Fig. 1a) at 13 JST on 1 April 2007.

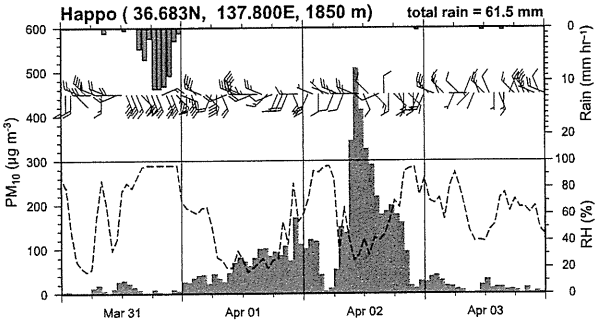

Fig. 6. Time series of PM_{10} (upward bar; μg m^{-3}), RH (dashed line; %), rain rate (downward bar; mm hr^{-1}), and wind (barb) at Happo (36.683°N, 137.800°E; 1850 m), Japan.

also detected this feature as a cloud. The cloud mask scheme for extremely high backscattering coefficients will be addressed in future algorithm improvements (Hagihara and Okamoto 2010; personal communication).

CloudSat/Cloud Profiling Radar cannot obtain an effective signal near the ground because surface clutter makes it difficult to detect low-level clouds along mountain slopes. To show the humidity conditions over mountains, Fig. 6 illustrates time series of PM_{10} and meteorological variables at Happo (z = 1850 m). After frontal rainfall, PM_{10} increased with time on 1 April. During

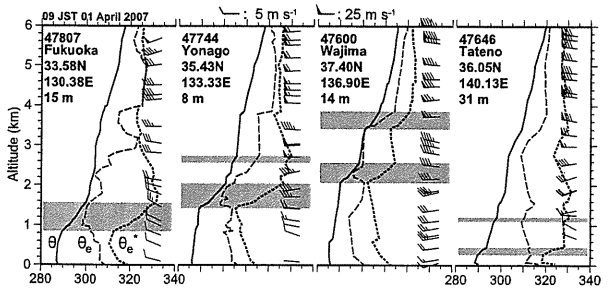

Fig. 7. Vertical profiles of θ (solid), θ_e (dashed), and θ_e* (dotted) at four rawinsonde sites at 09 JST on 1 April. Shading represents temperature inversions ($\Delta T/\Delta z > 0$; $\Delta z \geq 100$ m only).

the day, a fairly dry air (RH < 30%) was observed under westerly wind conditions. Dry conditions were also observed at other observatories over mountainous areas during the day (not shown). These results suggest that wet deposition was not the primary reason for the temporal delay of SPM increase in Kanto.

Finally, we consider the possibility of indirect dust transport. The most important point for indirect transport is the vertical stability above severe dust layers. In the TAD-2007 case, the severe dust layers over the windward side of mountains were capped by temperature inversions. Figure 7 shows vertical profiles of θ, equivalent θ (θ_e), and saturated θ_e (θ_e*) at 09 JST on 1 April at four rawinsonde sites (see Fig. 1a). Strong temperature inversions were clearly found along the Sea of Japan coast. Although the heights of the inversion base increased with the eastward advance, θ at the inversion base was nearly the same ($\theta \approx 290$ K). Other lidar observations (Fukue, Nagasaki, and Matsue) upstream of Kanto also indicated that the severe dust layer was under the inversion base (not shown). The near surface dust layer in Kanto was also observed for $\theta < 290$ K airmasses under easterly wind conditions (Fig. 4b). Therefore, because the severe dust layer was trapped under strong temperature inversions and lower than the height of the mountains (approximately 2000 m), the main body of the dust layer could not have passed over the mountains.

5. Conclusions

During the TAD-2007 episode, the daytime SPM over Kanto remained low (~40 μg m^{-3}) on 1 April and then increased later in the late afternoon. The severe dust layer windward of the central mountains was confined to cold air ($\theta < 290$ K) and trapped by a strong temperature inversion (Figs. 4a and 7). A capped dust layer was also reported in previous studies (e.g., Murayama et al. 2001). In addition, because of the dry condition both in the low-level dust layer and aloft, there was no cloud condensation along the windward slope or rainfall over the mountains. These results indicate that the temporal delay of SPM increase over Kanto was mainly caused by the indirect transport of low-level dust around Japan's central mountain ranges.

While only a case study has been presented here, indirect Asian dust transport may occur frequently in Kanto (Takahashi et al. 2010). Hara et al. (2009) reported that Asian dust in a cold sector was confined within PBL and transported farther downstream by an advancing frontal system. The PBL confined dust also had dry air aloft, similar to the case of TAD-2007. To clarify the occurrence frequency of indirect transport and primary processes, further studies will be required using both long-term observational data analysis and numerical experiments with dust emission/transport models.

Acknowledgments

Comments and suggestions made by two reviewers are very helpful in improving the presentation of this paper. We thank Dr. Tsunematsu (Chiba Univ., Japan) for valuable comments. The operational air-quality monitoring dataset is obtained from the cooperative research project for photochemical oxidant and particulate matters (NIES, Japan). We would like to thank Dr. Y. Hagihara and Dr. H. Okamoto (RIAM, Kyushu Univ., Japan) for offering access of the merged datasets. This paper contributes to the Joint Research on Dust and Sandstorm under TEMM-WG1.

Supplement

Supplement 1 shows hourly animation of SPM concentrations and surface horizontal wind obtained from GPV-MSM.

References

Hagihara, Y., H. Okamoto, and R. Yoshida, 2010: Development of a combined CloudSat-CALIPSO cloud mask to show global cloud distribution. *J. Geophys. Res.*, **115**, D00H33, doi: 10.1029/2009JD012344.

Han, Z., H. Ueda, K. Matsuda, R. Zhang, K. Arao, Y. Kanai, and H. Hasome, 2004: Model study on particle size segregation and deposition during Asian dust events in March 2002. *J. Geophys. Res.*, **109**, D19205, doi:10.1029/2004JD004920.

Hara, Y., K. Yumimoto, I. Uno, A. Shimizu, N. Sugimoto, Z. Liu, and D. M. Winker, 2009: Asian dust outflow in the PBL and free atmosphere retrieved by NASA CALIPSO and an assimilated dust transport model. *Atmos. Chem. Phys.*, **9**, 1227–1239.

Minoura, H., K. Takahashi, J. C. Chow, and J. G. Watson, 2006: Multiyear trend in fine and coarse particle mass, carbon, and ions in downtown Tokyo, Japan. *Atmos. Environ.*, **40**, 2478–2487.

Murayama, T., N. Sugimoto, I. Uno, K. Kinoshita, K. Aoki, N. Hagiwara, Z. Liu, I. Matsui, T. Sakai, T. Shibata, K. Arao, B.-J. Sohn, J.-G. Won, S.-C. Yoon, T. Li, J. Zhou, H. Hu, M. Abo, K. Iokibe, R. Koga, and Y. Iwasaka, 2001: Ground-based network observation of Asian dust events of April 1998 in east Asia. *J. Geophys. Res.*, **106**, 18345–18359.

Park, S.-U., A. Choe, and M.-S. Park, 2010: Estimates of Asian dust deposition over the Asian region by using ADAM2 in 2007. *Sci. Total Environ.*, **408**, 2347–2356.

Shimizu, A., N. Sugimoto, I. Matsui, K. Arao, I. Uno, T. Murayama, N. Kagawa, K. Aoki, A. Uchiyama, and A. Yamazaki, 2004: Continuous observations of Asian dust and other aerosols by polarization lidars in China and Japan during ACE-Asia. *J. Geophys. Res.*, **109**, D19S17, doi:10.1029/2002JD003253.

Takahashi, H., H. Naoe, Y. Igarashi, Y. Inomata, and N. Sugimoto, 2010: Aerosol concentrations observed at Mt. Haruna, Japan, in relation to long-range transport of Asian mineral dust aerosols. *Atmos. Environ.*, **44**, 4638–4644.

Tsunematsu, N., H. Iwai, S. Ishii, M. Yasui, Y. Murayama, and K. Mizutani, 2009: Influence of surface-based stable layer development on Asian dust behavior over Tokyo. *Boundary-Layer Meteor.*, **131**, 263–275.

Yoshida, R., H. Okamoto, Y. Hagihara, and H. Ishimoto, 2010: Global analysis of cloud phase and ice crystal orientation from Cloud-Aerosol Lidar and Infrared Pathfinder Satellite Observation (CALIPSO) data using attenuated backscattering and depolarization ratio. *J. Geophys. Res.*, **115**, D00H32, doi:10.1029/2009JD012334.

Yumimoto, K., I. Uno, N. Sugimoto, A. Shimizu, Z. Liu, and D. M. Winker, 2008: Adjoint inversion modeling of Asian dust emission using lidar observations. *Atmos. Chem. Phys.*, **8**, 2869–2884.

Manuscript received 15 November 2010, accepted 17 February 2011
SOLA: http://www.jstage.jst.go.jp/browse/sola

Toxicology and Applied Pharmacology 254 (2011) 48–55

Contents lists available at ScienceDirect

Toxicology and Applied Pharmacology

journal homepage: www.elsevier.com/locate/ytaap

A possible mechanism for 2,2′,4,4′,5,5′-hexachlorobiphenyl-mediated decrease in serum thyroxine level in mice

Yoshihisa Kato [a,*], Mao Onishi [b], Koichi Haraguchi [c], Shinichi Ikushiro [d], Chiho Ohta [e], Nobuyuki Koga [e], Tetsuya Endo [f], Shizuo Yamada [b], Masakuni Degawa [b]

[a] Kagawa School of Pharmaceutical Sciences, Tokushima Bunri University, Sanuki, Kagawa 769-2193, Japan
[b] School of Pharmaceutical Sciences and Global Center of Excellence Program, University of Shizuoka, Shizuoka 422-8526, Japan
[c] Daiichi College of Pharmaceutical Sciences, Fukuoka 815-8511, Japan
[d] Faculty of Engineering, Toyama Prefectural University, Toyama 939-0398, Japan
[e] Faculty of Nutritional Sciences, Nakamura Gakuen University, Fukuoka 814-0198, Japan
[f] Faculty of Pharmaceutical Sciences, Health Science University of Hokkaido, Hokkaido 061-0293, Japan

ARTICLE INFO

Article history:
Received 25 December 2010
Revised 23 April 2011
Accepted 25 April 2011
Available online 4 May 2011

Keywords:
2,2′,4,4′,5,5′-Hexachlorobiphenyl
UDP-glucuronosyltransferase
Thyroxine
Mice

ABSTRACT

Serum total thyroxine (T_4) level was markedly decreased, without significant increases in the levels of hepatic T_4–UDP-glucuronosyltransferase (T_4–UGT) and serum thyroid-stimulating hormone, 3 days after treatment with 2,2′,4,4′,5,5′-hexachlorobiphenyl (CB153) (100 mg/kg, ip) in both 2,3,7,8-tetrachlorodibenzo-*p*-dioxin (TCDD)-sensitive C57BL/6 and TCDD-resistant DBA/2 mice. Likewise, in either strain of mice, no CB153-mediated changes in the binding levels of [^{125}I]T_4 to serum proteins, such as transthyretin, albumin, and thyroxine binding globulin, were observed, while in CB153-pretreated C57BL/6 mice, but not in CB153-pretreated DBA/2 mice, the levels of biliary [^{125}I]T_4 and [^{125}I]T_4–glucuronide at 90–120 min after injection of [^{125}I]T_4 slightly increased, as compared with those in the corresponding control mice. Concerning tissue distribution of [^{125}I]T_4, liver-selective increases in the [^{125}I]T_4 accumulation by CB153-pretreatment were observed in both C57BL/6 and DBA/2 mice, and the hepatic levels of [^{125}I]T_4 in the C57BL/6 and DBA/2 mice became more than 44% and 34% of the [^{125}I]T_4 dosed, respectively. The present findings indicated that the CB153-mediated decreases in the level of serum total T_4 in C57BL/6 and DBA/2 mice occur mainly through an increase in the accumulation of T_4 in the liver.

Introduction

Studies on the toxicities of polychlorinated biphenyls (PCBs) (Safe, 1990; Brouwer et al., 1999), such as body weight loss, endocrine disruption, teratogenicity, carcinogenicity, and the impairment of the reproductive and immune systems, have been performed over the last 40 years. Furthermore, Yusho (oil disease) patients are reported to show various symptoms such as acneform, eruptions, the hypersecretion of meibomian glands, and the hyperpigmentation of face, eyelids and gingiva (Kuratsune et al., 1972).

PCBs consist of a series of 209 individual congeners varying in the number and position of substituent chlorine in a biphenyl structure and are classified as non-*ortho* PCB congner, di-*ortho* PCB congener, and mono-*ortho* PCB congener on the basis of the induction pattern of hepatic drug-metabolizing enzymes, including cytochrome P450 (CYP) and UDP-glucuronosyltransferase (UGT) family enzymes (McFarland and Clarke, 1989). 3,3′,4,4′,5-Pentachlorobiphenyl (CB126), a TCDD-type inducer, induces the CYP1A and UGT1A subfamily enzymes in the liver (Bock, 1991; Kato et al., 2010a), while 2,2′,4,4′,5,5′-hexachlorobiphenyl (CB153) (Fig. 1) is considered as a PB-type inducer (McFarland and Clarke, 1989), which induces the CYP2B and UGT2B subfamily enzymes (Bock, 1991).

PCB congeners, such as CB126, CB153, 2,3,3′,4,4′,5-hexachlorobiphenyl (CB156), and 2,3′,4,4′,5-pentachlorobiphenyl (CB118), are well known to decrease the levels of serum thyroid hormone and to increase the activities of hepatic drug-metabolizing enzymes in rats and mice (Craft et al., 2002; Desaulniers et al., 1999; Ness et al., 1993; Van Birgelen et al., 1995). As a possible mechanism for the PCB-mediated decrease in serum thyroid hormone, increases in hepatic UGTs, especially UGT1A1 (Visser, 1996), responsible for thyroid hormone metabolism and in the release of thyroxine (T_4) from a complex of T_4–serum transport protein, transthyretin (TTR), have been proposed (Craft et al., 2002; Brouwer et al., 1998). In addition, some of hydroxylated PCB metabolites show a high binding affinity for

Abbreviations: CB153, 2,2′,4,4′,5,5′-hexachlorobiphenyl; PCB, polychlorinated biphenyl; T_4, thyroxine; T_3, triiodothyronine; TTR, transthyretin; TSH, thyroid-stimulating hormone; UGT, UDP-glucuronosyltransferase; HPLC, high-performance liquid chromatography; TBG, thyroxine binding protein.

* Corresponding author at: Kagawa School of Pharmaceutical Sciences, Tokushima Bunri University, 1314-1 Shido, Sanuki, Kagawa 769-2193, Japan. Fax: +81 87 894 01 81.
E-mail address: kato@kph.bunri-u.ac.jp (Y. Kato).

0041-008X/$ – see front matter © 2011 Elsevier Inc. All rights reserved.
doi:10.1016/j.taap.2011.04.020

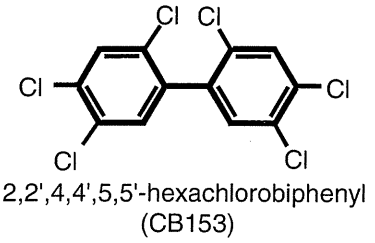

Fig. 1. Chemical structure of 2,2′,4,4′,5,5′-hexachlorobiphenyl (CB153).

serum TTR rather than do the parent PCB (Brouwer et al., 1998; Lans et al., 1993; Ucán-Marín et al., 2009).

However, we have demonstrated that a commercial PCB mixture, the Kanechlor-500 (KC500)-mediated decrease occurs through increased accumulation of T_4 in several tissues, especially the liver, rather than an increase in hepatic T_4–UGT activity (Kato et al., 2007), and further indicated that decrease in serum T_4 level by CB126 occurs not only through the induction of hepatic T_4–UGT but also through the enhanced accumulation of hepatic T_4 along with development of liver hypertrophy (Kato et al., 2010a). More recently, we have found that phenobarbital (PB)-mediated decreases in the serum T_4 level in mice, hamsters, and rats occur mainly through an increase in the accumulation level of T_4 in the liver (Kato et al., 2010b). Furthermore, since the magnitude of induction of T_4–UGT is not well correlated with the magnitude of decrease in the serum total T_4 level in the rodent exposed to CB153, a PB-type inducer of drug-metabolizing enzymes (Craft et al., 2002), an exact mechanism for the chemical-mediated decrease in serum T_4 level remains unclear.

In the present work, therefore, to further clarify an exact mechanism for the decrease in the serum total T_4 level in the mice treated with CB153, a PB-type inducer of drug-metabolizing enzymes, we examined whether or not there is a strain difference in CB153-mediated decrease of serum total T_4 level between C57BL/6 and DBA/2 mice, which are responsive and non-responsive mice, respectively, to the chemical-mediated induction of T_4–UGTs. The results indicated that there is no strain difference in the pattern of the CB153-mediated decrease in serum total T_4 level. Namely, the CB153-mediated decreases in the serum total T_4 level in both strains of mice were clarified to be primarily dependent on the enhanced accumulation of T_4 in the liver and slightly on the increase in excretion amounts of biliary T_4 and T_4–glucuronide.

Materials and methods

Chemicals

Panacete 810 (medium-chain triglycerides) was purchased from Nippon Oils and Fats Co. Ltd. (Tokyo, Japan). The [^{125}I]T_4, radiolabelled at the 5′-position of the outer ring, was obtained from PerkinElmer Life and Analytical Sciences (Waltham, MA). CB153 were purchased from Cambridge Isotope Laboratories, Inc. (MA, USA). All the other chemicals used herein were obtained commercially in appropriate grades of purity.

Animal treatments

Male C57BL/6 mice (16–31 g) and the DBA/2 mice (17–29 g) were obtained from Japan SLC., Inc. (Shizuoka, Japan). Male C57BL/6 and DBA/2 mice were housed three or four per cage with free access to commercial chow and tap water, maintained on a 12-h dark/light cycle (8:00 AM to 8:00 PM light) in an air-controlled room (temperature, 24.5 ± 1 °C and humidity, 55 ± 5%), and handled with animal care under the guidelines of the University of Shizuoka (Shizuoka, Japan). Mice received a single ip injection of CB153 (12.5, 25, 50, 100 or 200 mg/kg) dissolved in Panacete 810 (5 ml/kg). Control animals were treated with vehicle alone (5 ml/kg).

In vivo study

Mice were killed by decapitation 3 days after the administration of CB153. The thyroid gland and liver were removed and weighed. Hepatic microsomes were prepared according to the method of Kato et al. (1995) and stored at −85 °C until use. Blood was collected from each animal between 10:30 and 11:30 AM. After clotting at room temperature, serum was separated by centrifugation and stored at −50 °C until use.

Analysis of serum hormones. Levels of total T_4, total triiodothyronine (T_3), and thyroid-stimulating hormone (TSH) were measured by radioimmunoassay using Total T4 kit (Diagnostic Products Corporation; Los Angeles, CA), T-3 RIABEAD (Dainabot Co., Ltd., Tokyo, Japan), and the rTSH [^{125}I] Biotrak assay system (GE Healthcare UK, Ltd., Little Chalfont, Buckinghamshine, UK), respectively. These assays were performed in accordance with the manufacturer's instructions. In the intra-assay variation coefficients for the total T_4 and total T_3 assays in this study were 5.7% and 3.1%, respectively, and their detection limits were 0.25 μg/dl and 0.1 ng/ml, respectively.

Hepatic microsomal enzyme assays. The amount of hepatic microsomal protein was determined by the method of Lowry et al. (1951) with bovine serum albumin as a standard. Microsomal *O*-dealkylase activities of 7-benzyloxy-, 7-ethoxy-, and 7-pentoxyresorufins were determined by the method of Burke et al. (1985). The activity of microsomal UGT toward T_4 (T_4–UGT activity) was determined by the method of Barter and Klaassen (1992).

Western blot analysis. Western blot analyses for microsomal UGT isoforms were performed by the method of Luquita et al. (2001) using polyclonal anti-peptide antibodies against the common region of rat UGT1A isoforms and specific antibody against rat UGT1A1 (Ikushiro et al., 1995, 1997). Mouse Ugt1a1, which corresponds to rat UGT1A1, was measured by use of an ECL detection kit (GE Healthcare UK, Ltd.), and the level of each protein was determined densitometrically with LAS-1000 (Fuji Photo Film. Co., Ltd., Tokyo, Japan).

Ex vivo study

At 3 days after treatment with CB153, the mice were anesthetized with saline solution (2 ml/kg) containing sodium pentobarbital (25 mg/ml) and potassium iodide (1 mg/ml). The femoral artery was cannulated (polyethylene tube SP8, Natsume Inc., Tokyo, Japan) and primed with heparinized saline (33 units/ml), and then the animal's body was warmed to 37 °C. Fifteen minutes later, the mice received a single i.v. injection of 1.5 μCi [^{125}I]T_4 (0.1 ml) dissolved in saline containing 10 mM NaOH and 1% normal mouse serum. In addition, since bile was collected within 2.25 h after pentobarbital administration, pentobarbital-mediated induction of the enzymes responsible for T_4 metabolism is little expected.

Biliary excretion of total [^{125}I]T_4 and [^{125}I]T_4 glucuronide. After the administration of [^{125}I]T_4, bile was collected on ice for 2 h at 30 min intervals. Bile volume was determined gravimetrically. The amounts of total [^{125}I]T_4 and [^{125}I]T_4 glucuronide in bile were determined by the method of Vansell and Klaassen (2001). In brief, an aliquot (10 μl) of each bile sample was used for determining total [^{125}I]T_4 level by a gamma-counter (Cobra II Auto-Gamma 5002; PerkinElmer Life and Analytical Sciences), and the assay was performed in duplicate. To measure the amount of [^{125}I]T_4 glucuronide in bile, a portion (10 μl) of each bile sample was added 2 volume methanol and stored at −20 °C for 1 h to precipitate protein. After the mixture was centrifuged at

12,000 *g* (4 °C) for 10 min, and the resultant supernatant was collected for high-performance liquid chromatography (HPLC) analysis. The HPLC analysis was performed using a ChromSpher C18 column (10×0.3 cm) (Chrompack, Inc., Raritan, NJ) in combination with both a ChromSep reverse-phase guard column (10×2 mm) (Chrompack, Inc.) and an Adsorbosphere C18 reverse-phase guard column (7.5×4.6 mm) (Alltech Associates, Inc., Deerfield, IL). A solution of 0.02 mM ammonium acetate (pH 4.0) containing 16–45% acetonitrile was used to elute [^{125}I]T_4 glucuronide; 16% of acetonitrile was used as a initial solution for 6 min, and then the elution solution was changed by a linear increase to 27% over 12 min, held for 4 min, followed by a linear increase to 45% over 5 min and held for 11 min. The level of biliary [^{125}I]T_4 glucuronide was determined by Radioisotope Detector 171 (Beckman Coulter, Inc. CA USA).

Analysis of [^{125}I]T_4 bound to serum proteins. The levels of serum [^{125}I]T_4–thyroxine binding globulin (TBG), [^{125}I]T_4–albumin, and [^{125}I]T_4–TTR complexes were determined according to the method of Davis et al. (1970). In brief, after the administration of [^{125}I]T_4, serum was prepared from a portion (0.08 ml) of blood, which was sampled from the artery at the indicated times, and the serum was stored at −50 °C until use. Serum was diluted in 100 mM phosphate buffer (pH 7.4) containing 1 mM EDTA, 1 mM dithiothreitol, and 30% glycerol, and the diluted serum was subjected to electrophoresis on 4–20% gradient native polyacrylamide gels PAG Mid "Daiichi" 4/20 (Daiichi Pure Chemicals Co., Ltd., Tokyo, Japan). The electrophoresis was performed at 4 °C for 11 h at 20 mA in the 0.025 M Tris buffer (pH 8.4) containing 0.192 M glycine. The human albumin and TTR, which were incubated with [^{125}I]T_4, were also applied on the gel as templates. After the electrophoresis, a gel was dried and radioautographed for 20 h at room temperature using Imaging Plate 2040 (Fuji Photo Film Co., Ltd., Japan). The levels of [^{125}I]T_4–TBG, [^{125}I]T_4–albumin, and [^{125}I]T_4–TTR in serum were determined by counting the corresponding gel fractions identified from Bio Imaging Analyzer (BAS-2000II IP Reader, Fuji Photo Film Co., Ltd., Japan).

Tissue distribution of [^{125}I]T_4. Tissue distribution of [^{125}I]T_4 was performed according to the modified method of Oppenheimer et al. (1968). In brief, at 5 min after administration of [^{125}I]T_4 to CB153-pretreated mice, cerebrum, cerebellum, pituitary gland, thyroid gland, sublingual gland, submandibular gland, thymus, heart, lung, liver, kidney, adreanal gland, spleen, testis, prostate gland, seminal vesicle, stomach, duodenum, jejunum, ileum, and caecum were removed and weighed. Radioactivities in the tissues were determined by a gamma-counter (Cobra II Auto-Gamma 5002; PerkinElmer Life and Analytical Sciences).

Statistics

The data obtained were statistically analyzed according to Student's *t* test or Dunnett's test after analysis of variance. In addition, the amount of biliary [^{125}I]T_4 glucuronide and the binding level of [^{125}I]T_4 bound to serum proteins were statistically analyzed according to Newman–Keuls' test after analysis of variance.

Results

Serum hormone levels

We first examined the changes in the level of serum total T_4 at 2, 3, 4, 5, 6, 7 and 8 days after the treatment with CB153 (200 mg/kg), and then day 3 after the chemical treatment was selected as a suitable time, because serum total T_4 level has reached minimum at day 3, and the decreased levels were maintained up to day 8. Subsequently, the dose effect of CB153 on the level of serum total T_4 was examined in C57BL/6 mice 3 days after the chemical treatment (Fig. 2). Serum total

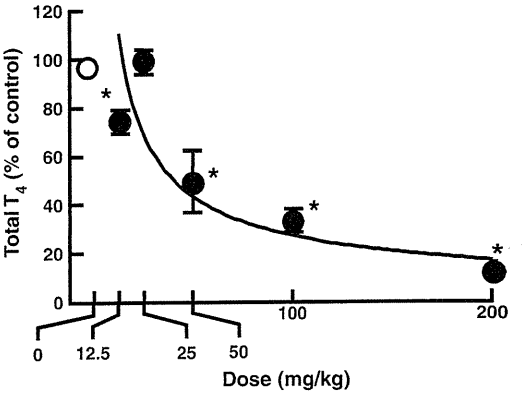

Fig. 2. Dose–effect of CB153 on the level of the serum total T_4 in C57BL/6 mice. Mice were killed 3 days after the ip administration of CB153 at the various doses indicated, and the level of the serum total T_4 was measured as described in Materials and methods. Constitutive total T_4 level: 2.74 ± 0.23 μg/dl ($n = 4$). Each point represents the mean ± S.E. (vertical bar) for four to five mice. *$P<0.05$, significantly different from the control.

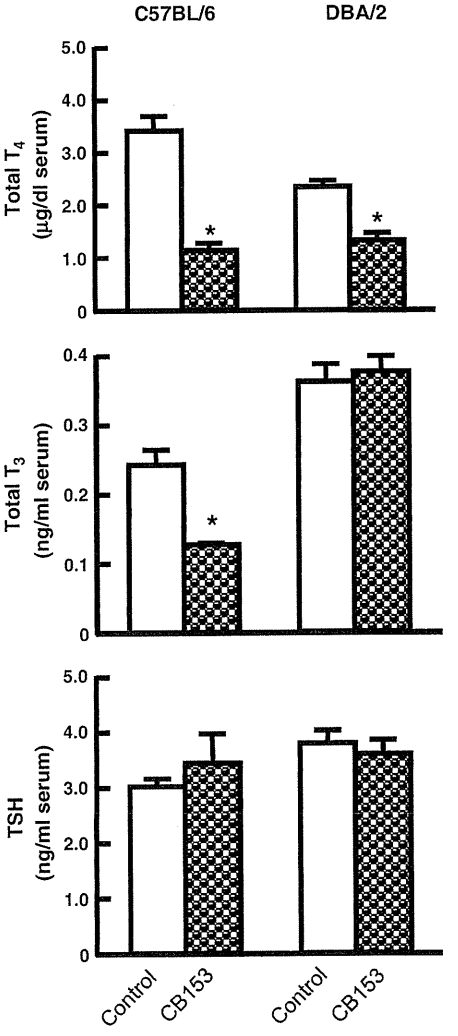

Fig. 3. Effects of CB153 on the levels of serum total T_4, total T_3, and TSH. Animals were killed 3 days after the administration of CB153 (100 mg/kg), and levels of serum thyroid hormones were measured, as described in Materials and methods. Each column represents the mean ± S.E. (vertical bar) for four to five animals. *$P<0.05$, significantly different from each control.

Table 1
Effects of CB153 on the activity of hepatic microsomal alkoxyresorufin *O*-dealkylases in C57BL/6 and DBA/2 mice.

O-Dealkylase of alkoxyresolfin	C57BL/6		DBA/2	
	Control	CB153	Control	CB153
7-Ethoxy-	0.17 ± 0.02	0.27 ± 0.04*	0.10 ± 0.004	0.15 ± 0.009*
7-Benzyloxy-	0.12 ± 0.003	0.89 ± 0.13*	0.04 ± 0.003	0.33 ± 0.05*
7-Pentoxy-	0.03 ± 0.004	0.11 ± 0.02*	0.02 ± 0.004	0.06 ± 0.01*

Animals were killed 3 days after the administration of CB153 (100 mg/kg). The activities of alkoxyresolfin *O*-dealkylase are represented as nmol of the resolfin formed/mg protein/min. Data represent the mean ± S.E. for four to five mice. *$P<0.05$, significantly different from each control.

T_4 level was significantly decreased by the treatment with CB153 at doses of over 12.5 mg/kg, and the decreases occurred in a dose-dependent fashion up to 200 mg/kg. On the basis of the results of the preliminary experiments, the suitable dose (100 mg/kg) and time (3 days after the dosing) were determined.

The effects of CB153 on the levels of serum thyroid hormones were examined in C57BL/6 and DBA/2 mice (Fig. 3). Serum total T_4 level 3 days after the CB153 treatment was markedly decreased in both C57BL/6 and DBA/2 mice. The magnitude of the decrease in the level of serum total T_4 in C57BL/6 mice was greater than that in DBA/2 mice, although absolute level of the hormone after CB153 treatment was almost the same in both strains of mice. Serum total T_3 level 3 days after the treatment with CB153 was significantly decreased in C57BL/6 mice, but not in DBA/2 mice (Fig. 3). On the other hand, no significant increase in the level of serum TSH by the CB153 treatment was observed in either strain of mice (Fig. 3).

Hepatic drug-metabolizing enzymes

Effects of CB153 on hepatic microsomal activities of ethoxyresorufin *O*-dealkylase (Cyp1a1/2), benzyloxyresorufin *O*-dealkylase (Cyp2b1/2 and Cyp3a1/2), and pentoxyresorufin *O*-dealkylase (Cyp2b1/2) were examined in C57BL/6 and DBA/2 mice. Treatments of C57BL/6 and DBA/2 mice with CB153 resulted in significant increases in hepatic microsomal enzyme activities: 1.6- and 1.5-fold for ethoxyresorufin *O*-dealkylase activity, respectively; 7.4- and 8.3-fold for benzyloxyresorufin *O*-dealkylase activity, respectively; and 3.7- and 3.0-fold for pentoxyresorufin *O*-dealkylase activity, respectively (Table 1).

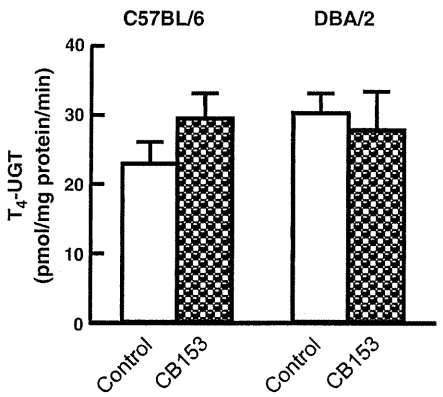

Fig. 4. Effect of CB153 on hepatic microsomal T_4-UGT activity. Hepatic microsomes from individual animals were used for T_4-UGT enzyme assay, as described in Materials and methods. Each column represents the mean ± S.E. (vertical bar) for four animals.

Hepatic T_4-UGT

Since T_4-glucuronidation is primarily mediated by hepatic UGT1A1 and UGT1A6 in the rat liver (Visser, 1996), we first examined the effects of CB153 on hepatic microsomal T_4-UGT activity in C57BL/6 and DBA/2 mice. No significant increase in the activity of hepatic T_4-UGT was observed in either strain of mice (Fig. 4).

Furthermore, the effects of CB153 on the amounts of the proteins responsible for the T_4-UGTs, such as total Ugt1a and Ugt1a1, were examined by Western blot analysis (Fig. 5A). The amounts of hepatic

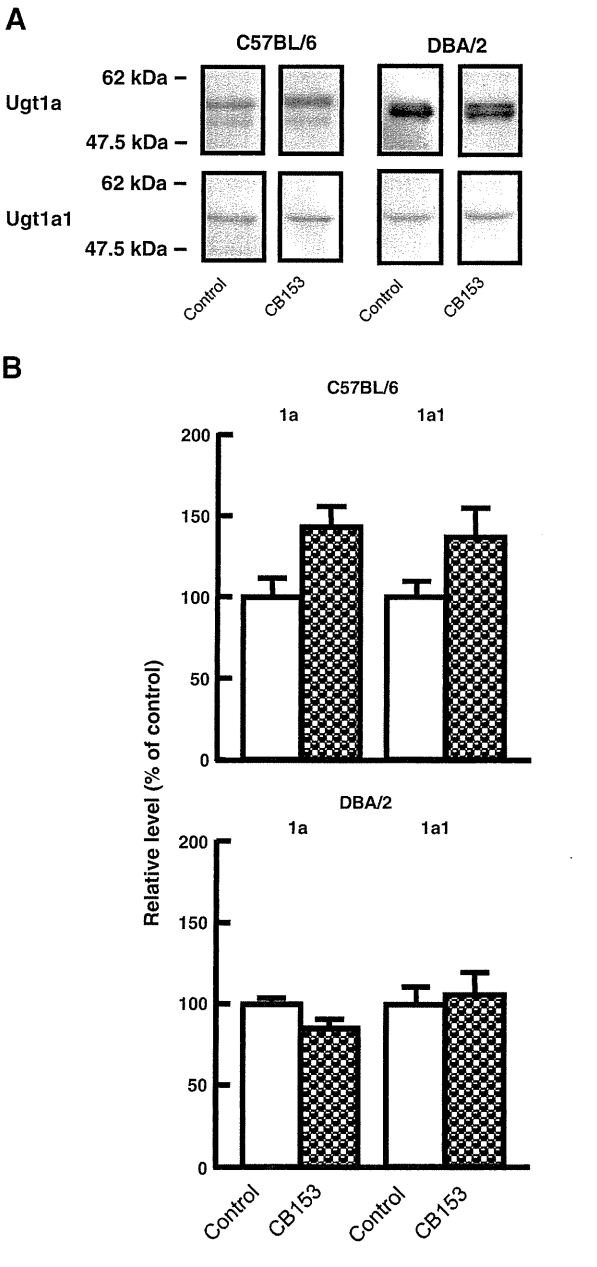

Fig. 5. The representative Western blot patterns for hepatic microsomal Ugt isoforms (A) and the amounts of their isoforms (B) in CB153-treated mice. Hepatic microsomes from individual animals were used for Western blot analysis, as described in Materials and methods. The separated bands responsible for Ugt isoforms, which are shown in (A), were densitometrically quantified as described in Materials and methods. The data are represented as the mean ± SE (vertical bar) for four animals (B).

Ugt1a and Ugt1a1 enzyme proteins were not significantly changed by CB153 treatment in either strain of mice (Fig. 5B).

In addition, the amounts of biliary [^{125}I]T_4 and [^{125}I]T_4–glucuronide after i.v. injection of [^{125}I]T_4 were slightly increased by CB153-pretreatment in C57BL/6 mice, but not in DBA/2 mice (Fig. 6).

Serum proteins bound to [^{125}I]T_4

The effects of CB153 on the binding of [^{125}I]T_4 to serum proteins, such as TTR, albumin, and TBG, were examined in C57BL/6 and DBA/2 mice. No CB153-mediated change in the binding level of [^{125}I]T_4 to each serum protein after [^{125}I]T_4 administration was observed in either strain of mice (Fig. 7). Serum concentrations of CB153 and its hydroxylated metabolite, 3-OH-2,2′,4,4′,5,5′-hexachlorobiphenyl, were 3.39 and 0.32 μg/ml, respectively, in the CB153-treated C57BL/6 and, 1.08 and 0.02 μg/ml, respectively, in the CB153-treated DBA/2 mice. In addition, these chemicals were not detected in the CB153-untreated (control) C57BL/6 and DBA/2 mice.

Tissue distribution of [^{125}I]T_4

We first determined the suitable time for the assessment of the tissue distribution of [^{125}I]T_4 after [^{125}I]T_4-treatment. In brief, a portion of [^{125}I]T_4 (15 μCi/ml) was intravenously administered to mice, and the radioactivities in various tissues were measured at 5 and 60 min after the [^{125}I]T_4-administration. At both 5 and 60 min after the administration, the accumulation levels of [^{125}I]T_4 were the highest in the liver among all the tissues examined, and the accumulation levels of [^{125}I]T_4 in the liver at 5 min and 60 min were 31% and 22% of the [^{125}I]T_4 dosed, respectively. In addition, the accumulation levels of stomach and intestine were 0.9% and 2.5% of the [^{125}I]T_4 dosed, respectively, at 5 min later, and their levels were slightly increased to 3% and 5% of the [^{125}I]T_4 dosed, respectively, at 60 min later. Considering a liver-selective accumulation of [^{125}I]T_4, the tissue distribution of [^{125}I]T_4 was assayed at 5 min later.

Effects of CB153-pretreatment on the tissue distribution level of [^{125}I]T_4 were examined in C57BL/6 and DBA/2 mice. In the control C57BL/6 and DBA/2 mice, the accumulation of [^{125}I]T_4 was the highest in the liver among all the tissues examined (Fig. 8). In both strains of mice, pretreatment with CB153 resulted in an increase in the level of hepatic total [^{125}I]T_4, and the more than 44% and 34% of the [^{125}I]T_4 dosed were accumulated in the liver of C57BL/6 and DBA/2 mice, respectively (Fig. 8). Furthermore, the accumulation levels per gram liver in the CB153-pretreated C57BL/6 and DBA/2 were significantly increased to 1.41- and 1.23-times, respectively, as compared with those in the corresponding control animals. In addition, significant decrease in accumulation of [^{125}I]T_4 was observed in the heart, testis, and stomach in CB153-pretreated C57BL/6 mice (Fig. 8). In either strain of mice, no significant increases in the accumulation levels of [^{125}I]T_4 by CB153-pretreatment were observed in any extrahepatic tissues examined. Furthermore, no significant changes in the weights of the liver and thyroid gland after CB153-treatment were observed in either strain of mice (data not shown).

Discussion

In the present study, we demonstrated that treatment with CB153 resulted in significant decreases in the level of serum total T_4 in both C57BL/6 and DBA/2 mice. Furthermore, we herein indicated that CB153-mediated decreases in serum T_4 in C57BL/6 and DBA/2 mice occur mainly through an increase in the accumulation level of T_4 in the liver.

As a possible explanation for a TCDD-type PCB-induced decrease in serum thyroid hormones, hepatic T_4–UGT-dependent mechanism was considered, because T_4–UGT inducers, such as TCDD and CB126, have strong activities for decreasing serum total thyroid hormones in rats (Schuur et al., 1997; Van Birgelen et al., 1995). However, the T_4–UGT activity modified by CB153 is not necessarily correlated with a change in the level of serum total T_4 in both rats and mice (Craft et al., 2002). In this study, no significant changes in the amount and activity of

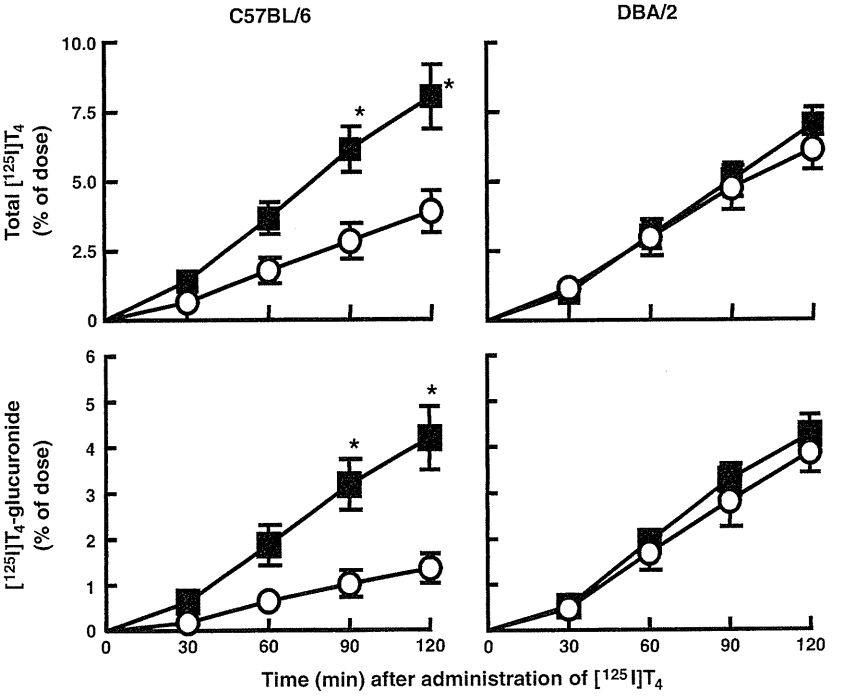

Fig. 6. Effects of CB153 on amounts of the biliary total [^{125}I]T_4 and [^{125}I]T_4–glucuronide. The bile was collected at 30-min intervals after the i.v. administration of [^{125}I]T_4, and amounts of the biliary total [^{125}I]T_4 and [^{125}I]T_4–glucuronide were measured as described in Materials and methods. Each point represents the mean ± S.E. (vertical bar) for four mice. *$P<0.05$, significantly different from each control. —○—, control; —■—, CB153.

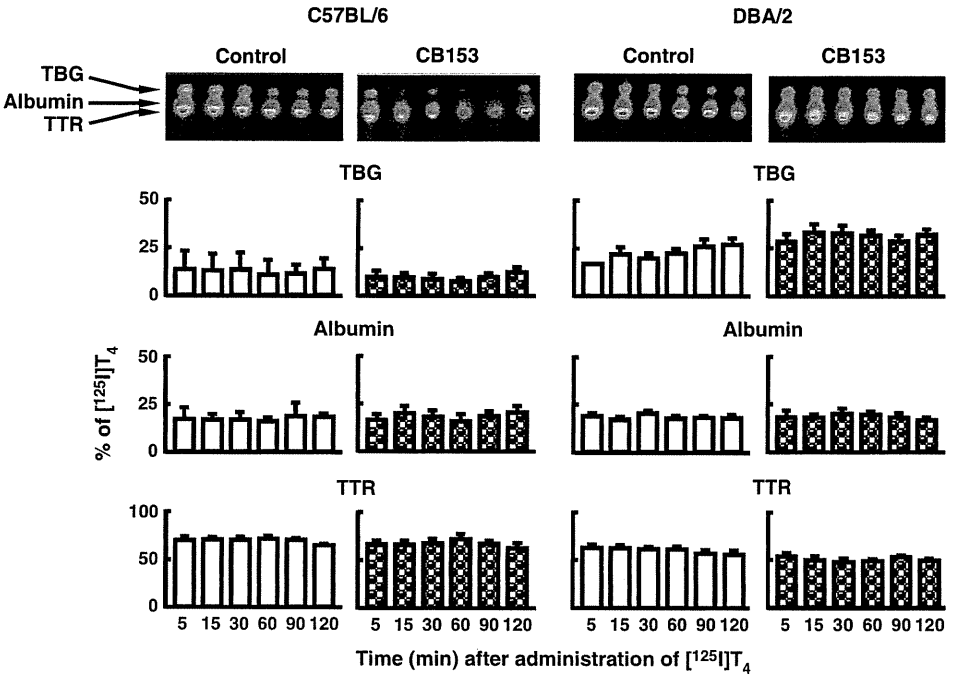

Fig. 7. Effects of CB153 on the amounts of the [^{125}I]T_4 bound to serum proteins in mice. The amounts of the [^{125}I]T_4 bound to the serum proteins 5 min after [^{125}I]T_4-administration were assessed by the method as described in Materials and methods. Each column represents the mean ± S.E. (vertical bar) for four to five animals.

hepatic T_4–UGTs, such as Ugt1a and Ugt1a1, by CB153 treatment were observed in either strain of mice, although the amounts of the biliary [^{125}I]T_4 and [^{125}I]T_4–glucuronide after i.v. injection of [^{125}I]T_4 slightly increased in the CB153-pretreated C57BL/6 mice, but not in the CB153-pretreated DBA/2 mice, as compared with the corresponding controls (Table 2). Such strain difference between C57BL/6 and DBA/2 mice in the excretion of the biliary [^{125}I]T_4 and [^{125}I]T_4–glucuronide might be dependent on the difference in the activity of the transporter responsible for excretion to the bile duct, because it has been reported that T_4 homeostasis are regulated by several transporters responsible for the excretion of the T_4 and T_4–glucuronide to the bile duct (Abe et al., 1999; Friesema et al., 1999, 2001, 2005; Lecureux et al., 2009; Pizzagalli et al., 2002).

In CB153-pretreated mice, more than 34% of the [^{125}I]T_4 dosed were accumulated in the liver, strongly suggesting that the decrease in the level of serum total T_4 in CB153-treated mice occurs mainly through the increase in a liver-selective accumulation of T_4. As a possible mechanism for CB153-mediated enhancement of T_4 accumulation in the liver, a TTR-associated pathway might be considered, because PCB and its hydroxylated metabolites act as the competitors

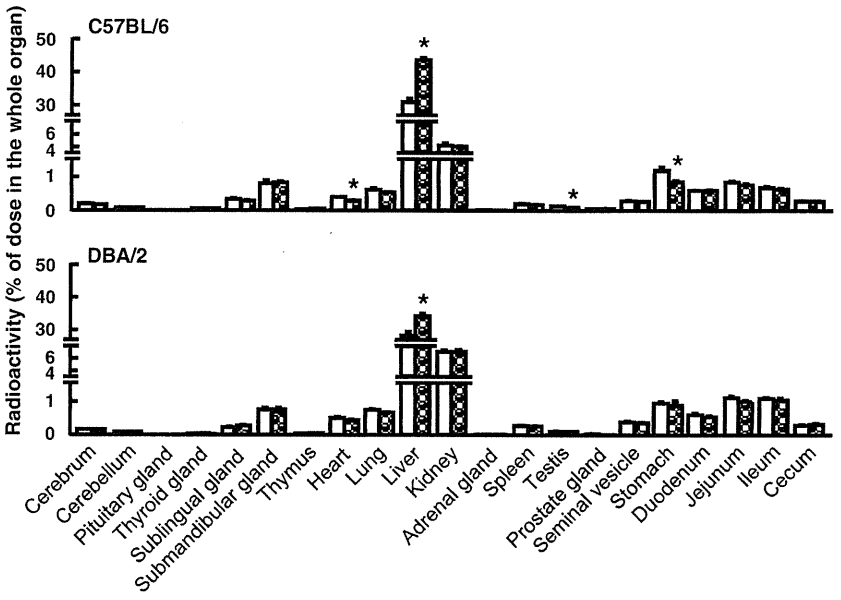

Fig. 8. Tissue distribution of [^{125}I]T_4 after the administration of [^{125}I]T_4 to CB153-pretreated mice. Three days after CB153-pretreatment, [^{125}I]T_4 was administered to mice, and after 5 min of the administration, the radioactivity in each tissue was measured, as described in Materials and methods. Each column represents the mean ± S.E. (vertical bar) for four animals. *$P<0.05$, significantly different from each control. □, control; ▩, CB153.

Table 2
Summary of the CB153-mediated effects.

Mice	Serum total T_4 (% of control)	Serum total T_3 (% of control)	TSH	Ugt1a	T_4–UGT Ugt1a1	Biliary total $[^{125}I]T_4$	Biliary $[^{125}I]T_4$–glucuronide	Accumulation of $[^{125}I]T_4$ in liver (% of dose)	Binding of $[^{125}I]T_4$ to serum TTR
C57BL/6	34%	52%	→[a]	→	→	↑[b]	↑	44%	→
DBA/2	56%	→	→	→	→	→	→	34%	→

[a] No significant change.
[b] Significant increase.

of T_4 forming T_4–TTR complex and because decrease in T_4–TTR complex leads to the increases in serum free T_4 and in T_4 uptake of the liver (Brouwer et al., 1998; Lans et al., 1993; Meerts et al., 2002; Kato et al., 2004). In addition, the concentrations of CB153 in the blood of Yusho patients are 10–1000-fold higher than those of serum thyroid hormones, suggesting that CB153 would competitively inhibit a T_4–TTR complex formation in the patients (Masuda, 2009).

However, the present study concerning the fate of serum T_4 using $[^{125}I]T_4$ indicated no CB153-mediated changes in the levels of the $[^{125}I]T_4$ bound to TTR, albumin, and TBG in either strain of mice. In addition, although some of the hydroxylated metabolites of PCBs are known to show higher capacities for binding to TTR (Brouwer et al., 1998; Lans et al., 1993; Ucán-Marín et al., 2009), the hydroxylated metabolites of CB153 were little detected in the serum in both the CB153-pretreated C57BL/6 and DBA/2 mice (data not shown). Accordingly, a TTR-associated pathway should not be considered as a mechanism for the CB153-mediated decrease in serum total T_4. Although an exact mechanism for the increase in the liver-selective $[^{125}I]T_4$ accumulation by CB153-pretreatment remains unclear, the liver-selective apparatus for T_4-transportation might exist. In addition, we confirmed herein that CB153 showed no ability to increase serum TSH, which is one of the factors regulating a serum thyroid hormone level, although some investigators have previously reported that PCBs have no effects on the levels of serum TSH and hepatic type-I iodothyronine deiodinase in rats (Hallgren et al., 2001; Hood et al., 1999; Liu et al., 1995; Kato et al., 2004).

In conclusion, we demonstrate in the present study that the CB153-mediated decrease in serum T_4 level in mice occurs mainly through the increase in accumulation of T_4 in the liver and slightly through an increase in the excretion of biliary $[^{125}I]T_4$ and $[^{125}I]T_4$–glucuronide. Further studies on the effects of PCBs, including CB153, on the function of hepatic T_4-transporters would be necessary for an understanding of an exact mechanism for the PCB-induced decrease in the serum T_4 level.

Funding

This work was supported in part by the Grant-in-Aid for Scientific Research (C) (no. 23510083, Y.K.) from Japan Society for the Promotion of Science.

Conflict of interest statement

The authors do not have any conflict of interest.

References

Abe, T., Kakyo, M., Tokui, T., Nakagomi, R., Nishio, T., Nakai, D., Nomura, H., Unno, M., Suzuki, M., Naitoh, T., Matsuno, S., Yawo, H., 1999. Identification of a novel gene family encoding human liver-specific organic anion transporter LST-1. J. Biol. Chem. 274, 17159–17163.

Barter, R.A., Klaassen, C.D., 1992. Rat liver microsomal UDP-glucuronosyltransferase activity toward thyroxine: characterization, induction, and form specificity. Toxicol. Appl. Pharmacol. 115, 261–267.

Bock, K.W., 1991. Roles of UDP-glucuronosyltransferases in chemical carcinogenesis. Crit. Rev. Biochem. Mol. Biol. 26, 129–150.

Brouwer, A., Morse, D.C., Lans, M.C., Schuur, A.G., Murk, A.J., Klasson-Wehler, E., Bergman, Å, Visser, T.J., 1998. Interactions of persistent environmental organohalogens with the thyroid hormone system: mechanisms and possible consequences for animal and human health. Toxicol. Ind. Health 14, 59–84.

Brouwer, A., Longnecker, M.P., Birnbaum, L.S., Cogliano, J., Kostyniak, P., Moore, J., Schantz, S., Winneke, G., 1999. Characterization of potential endocrine-related health effects at low-dose levels of exposure to PCBs. Environ. Health Perspect. 107, 639–649.

Burke, M.D., Thompson, S., Elcombe, C.R., Halpert, J., Haaparanta, T., Mayer, R.T., 1985. Ethoxy-, pentoxy- and benzyloxyphenoxazones and homologues: a series of substrates to distinguish between different induced cytochromes P-450. Biochem. Pharmacol. 34, 3337–3345.

Craft, E.S., DeVito, M.J., Crofton, K.M., 2002. Comparative responsiveness of hypothyroxinemia and hepatic enzyme induction in Long–Evans rats versus C57BL/6 J mice exposed to TCDD-like and phenobarbital-like polychlorinated biphenyl congeners. Toxicol. Sci. 68, 372–380.

Davis, P.J., Spaulding, S.W., Gregerman, R.I., 1970. The three thyroxine-binding proteins in rat serum: binding capacities and effects of binding inhibitors. Endocrinology 87, 978–986.

Desaulniers, D., Leingartner, K., Wade, M., Fintelman, E., Yagminas, A., Foster, W.G., 1999. Effects of acute exposure to PCBs 126 and 153 on anterior pituitary and thyroid hormones and FSH isoforms in adult Sprague Dawley male rats. Toxicol. Sci. 47, 158–169.

Friesema, E.C.H., Docter, R., Moerings, E.P.C.M., Stieger, B., Hagenbuch, B., Meier, P.J., Krenning, E.P., Hennemann, G., Visser, T.J., 1999. Identification of thyroid hormone transporter. Biochem. Biophys. Res. Commun. 254, 497–501.

Friesema, E.C.H., Docter, R., Moerings, E.P.C.M., Verrey, F., Krenning, E.P., Hennemann, G., Visser, T.J., 2001. Thyroid hormone transport by the heterodimeric human system L amino acid transporter. Endocrinology 142, 4339–4348.

Friesema, E.C.H., Jansen, J., Visser, T.J., 2005. Thyroid hormone transporters. Biochem. Soc. Trans. 33, 228–232.

Hallgren, S., Sinjari, T., Håkansson, H., Darnerud, P.O., 2001. Effects of polybrominated diphenyl ethers (PBDEs) and polychlorinated biphenyls (PCBs) on thyroid hormone and vitamin A levels in rats and mice. Arch. Toxicol. 75, 200–208.

Hood, A., Hashmi, R., Klaassen, C.D., 1999. Effects of microsomal enzyme inducers on thyroid-follicular cell proliferation, hyperplasia, and hypertrophy. Toxicol. Appl. Pharmacol. 160, 163–170.

Ikushiro, S., Emi, Y., Iyanagi, T., 1995. Identification and analysis of drug-responsive expression of UDP-glucuronosyltransferase family 1 (UGT1) isozyme in rat hepatic microsomes using anti-peptide antibodies. Arch. Biochem. Biophys. 324, 267–272.

Ikushiro, S., Emi, Y., Iyanagi, T., 1997. Protein–protein interactions between UDP-glucuronosyltransferase isozymes in rat hepatic microsomes. Biochemistry 36, 7154–7161.

Kato, Y., Haraguchi, K., Kawashima, M., Yamada, S., Masuda, Y., Kimura, R., 1995. Induction of hepatic microsomal drug-metabolizing enzymes by methylsulphonyl metabolites of polychlorinated biphenyl congeners in rats. Chem. Biol. Interact. 95, 257–268.

Kato, Y., Ikushiro, S., Haraguchi, K., Yamazaki, T., Ito, Y., Suzuki, H., Kimura, R., Yamada, S., Inoue, T., Degawa, M., 2004. A possible mechanism for decrease in serum thyroxine level by polychlorinated biphenyls in Wistar and Gunn rats. Toxicol. Sci. 81, 309–315.

Kato, Y., Ikushiro, S., Takiguchi, R., Haraguchi, K., Koga, N., Uchida, S., Sakaki, T., Yamada, S., Kanno, J., Degawa, M., 2007. A novel mechanism for polychlorinated biphenyl-induced decrease in serum thyroxine level in rats. Drug Metab. Dispos. 35, 1949–1955.

Kato, Y., Haraguchi, K., Kubota, M., Seto, Y., Okura, T., Ikushiro, S., Koga, N., Yamada, S., Degawa, M., 2010a. A possible mechanism for the decrease in serum thyroxine level by a 2,3,7,8-tetrachlorodibenzo-*p*-dioxin-like polychlorinated biphenyl congener, 3,3′,4,4′,5-pentachlorobiphenyl in mice. Drug Metab. Dispos. 38, 150–156.

Kato, Y., Suzuki, H., Haraguchi, K., Ikushiro, S., Ito, Y., Uchida, S., Yamada, S., Degawa, M., 2010b. A possible mechanism for the decrease in serum thyroxine level by phenobarbital in rodents. Toxicol. Appl. Pharmacol. 249, 238–246.

Kuratsune, M., Yoshimura, H., Matsuzaka, J., Yamaguchi, A., 1972. Epidemiologic study on Yusho, a poisoning caused by ingestion of rice oil contaminated with a commercial brand of polychlorinated biphenyls. Environ. Health Perspect. 46, 119–128.

Lans, M.C., Klasson-Wehler, E., Willemsen, M., Meussen, E., Safe, S., Brouwer, A., 1993. Structure-dependent, competitive interaction of hydroxy-polychlorobiphenyls, -dibenzo-*p*-dioxins and -dibenzofurans with human transthyretin. Chem.-Biol. Interact. 88, 7–21.

Lecureux, L., Dieter, M.Z., Nelson, D.M., Watson, L., Wong, H., Gemzik, B., Klaassen, C.D., Lehman-McKeeman, L.D., 2009. Hepatobiliary disposition of thyroid hormone in Mrp2-deficient TR– rats: reduced biliary excretion of thyroxine glucuronide does not prevent xenobiotic-induced hypothyroidism. Toxicol. Sci. 108, 482–491.

Liu, J., Liu, Y., Barter, R.A., Klaassen, C.D., 1995. Alteration of thyroid homeostasis by UDP-glucuronosyltransferase inducers in rats: a dose–response study. J. Pharmacol. Exp. Ther. 273, 977–985.

Lowry, O.H., Rosebrough, N.J., Farr, A.L., Randall, R.J., 1951. Protein measurement with the Folin phenol reagent. J. Biol. Chem. 193, 265–275.
Luquita, M.G., Catania, V.A., Pozzi, E.J.S., Veggi, L.M., Hoffman, T., Pellegrino, J.M., Ikushiro, S., Emi, Y., Iyanagi, T., Vore, M., Mottino, A.D., 2001. Molecular basis of perinatal changes in UDP-glucuronosyltransferase activity in maternal rat liver. J. Pharmacol. Exp. Ther. 298, 49–56.
Masuda, Y., 2009. Toxic effects of PCB/PCDF to human observed in Yusho and other poisonings. Fukuoka Acta Med. 100, 141–155.
McFarland, V.A., Clarke, J.U., 1989. Environmental occurrence, abundance, and potential toxicity of polychlorinated biphenyl congeners: considerations for a congener-specific analysis. Environ. Health Perspect. 81, 225–239.
Meerts, I.A.T.M., Assink, Y., Cenijn, P.H., van den Berg, J.H.J., Weijers, B.M., Bergman, Å., Koeman, J.H., Brouwer, A., 2002. Placental transfer of a hydroxylated polychlorinated biphenyl and effects on fetal and maternal thyroid hormone homeostasis in the rat. Toxicol. Sci. 68, 361–371.
Ness, D.K., Schantz, S.L., Moshtaghian, J., Hansen, L.G., 1993. Effects of perinatal exposure to specific PCB congeners on thyroid hormone concentrations and thyroid histology in the rat. Toxicol. Lett. 68, 311–323.
Oppenheimer, J.H., Bernstein, G., Surks, M.I., 1968. Increased thyroxine turnover and thyroidal function after stimulation of hepatocellular binding of thyroxine by phenobarbital. J. Clin. Invest. 47, 1399–1406.
Pizzagalli, F., Hagenbuch, B., Stieger, B., Klenk, U., Folkers, G., Meier, P.J., 2002. Identification of a novel human organic anion transporting polypeptide as a high affinity thyroxine transporter. Mol. Endocrinol. 16, 2283–2296.
Safe, S.H., 1990. Polychlorinated biphenyls (PCBs), dibenzo-*p*-dioxins (PCDDs), dibenzofurans (PCDFs), and related compounds: environmental and mechanistic considerations which support the development of toxic equivalency factors (TEFs). Crit. Rev. Toxicol. 21, 51–88.
Schuur, A.G., Boekhorst, F.M., Brouwer, A., Visser, T.J., 1997. Extrathyroidal effects of 2,3,7,8-tetrachlorodibenzo-*p*-dioxin on thyroid hormone turnover in male Sprague–Dawley rats. Endocrinology 138, 3727–3734.
Ucán-Marín, F., Arukwe, A., Mortensen, A., Gabrielsen, G.W., Fox, G.A., Letcher, R.J., 2009. Recombinant transthyretin purification and competitive binding with organohalogen compounds in two gull species (*Larus argentatus* and *Larus hyperboreus*). Toxicol. Sci. 107, 440–450.
Van Birgelen, A.P.J.M., Smit, E.A., Kampen, I.M., Groeneveld, C.N., Fase, K.M., van der Kolk, J., Poiger, H., van den Berg, M., Koeman, J.H., Brouwer, A., 1995. Subchronic effects of 2,3,7,8-TCDD or PCBs on thyroid hormone metabolism: use in risk assessment. Eur. J. Pharmacol. 293, 77–85.
Vansell, N.R., Klaassen, C.D., 2001. Increased biliary excretion of thyroxine by microsomal enzyme inducers. Toxicol. Appl. Pharmacol. 176, 187–194.
Visser, T.J., 1996. Pathways of thyroid hormone metabolism. Acta Med. Austriaca 23, 10–16.

Food and Chemical Toxicology 49 (2011) 2167–2171

Contents lists available at ScienceDirect

Food and Chemical Toxicology

journal homepage: www.elsevier.com/locate/foodchemtox

Transcellular transport of domoic acid across intestinal Caco-2 cell monolayers

Osamu Kimura [a], Yuichi Kotaki [b], Naoya Hamaue [a], Koichi Haraguchi [c], Tetsuya Endo [a,*]

[a] Faculty of Pharmaceutical Sciences, Health Sciences University of Hokkaido, 1757 Ishikari-Tobetsu, Hokkaido 061-0293, Japan
[b] School of Marine Biosciences, Kitasato University, Sanriku, Ofunato 022-0101, Japan
[c] Daiichi College of Pharmaceutical Sciences, 22-1 Tamagawa-Cho, Minami-Ku, Fukuoka 815-8511, Japan

ARTICLE INFO

Article history:
Received 18 October 2010
Accepted 1 June 2011
Available online 6 June 2011

Keywords:
Domoic acid
Intestinal transport
Caco-2 cells
Chloride ions
DIDS (4,4′-diisothiocyanostilbene-2,2′-disulfonic acid)

ABSTRACT

The intestinal absorption mechanism of domoic acid (DA) was investigated using Caco-2 cells. DA is a tricarboxylic amino acid that contains a glutamic acid moiety, and causes deficits in short-term memory by binding to glutamate receptors as an agonist of glutamic acid. Caco-2 cell monolayers cultured on permeable membranes were incubated with 100 μM DA on either the apical or basolateral side, and the transcellular transport of DA was measured. The transcellular transport of DA from the apical to basolateral side was about twofold that in the opposite direction. The transcellular transport of DA from the apical side was optimal at a neutral pH, and was temperature- and Cl^--dependent, but was Na^+-independent. Coincubation of DA with 4,4′-diisothiocyanostilbene-2,2′-disulfonic acid (DIDS), an anion exchange inhibitor, significantly decreased the apical-to-basolateral transport of DA by 48%, and coincubation with probenecid (a non-specific anion transport inhibitor) significantly decreased the transport of DA by 31%. In contrast, coincubation with glutamic acid, succinic acid (a dicarboxylic acid), or citric acid (a tricarboxylic acid) did not decrease the transport of DA. These results suggest that the apical-to-basolateral transport of DA across the Caco-2 cell monolayers is mediated by DIDS-sensitive anion transporters.

1. Introduction

Domoic acid (DA) is a potent excitotoxin produced by various marine algae and diatoms, and it has been found in marine wildlife throughout the world via the food web (Lefebvre and Robertson, 2010). DA is a tricarboxylic amino acid that contains glutamic acid moiety, and causes deficits in short-term memory by binding to glutamate receptors in the hippocampus as an agonist of glutamic acid (Wright et al., 1989; Hampson et al., 1992; Lefebvre and Robertson, 2010).

As most studies on DA using experimental animals have focused on the mechanisms of neurotoxicity, limited information is available on the intestinal absorption, distribution, metabolism, and excretion (ADME) of DA after ingestion. Truelove and Iverson (1994) investigated the pharmacokinetics of DA in monkeys and rats after intravenous dosing, and reported the rapid excretion of DA: the plasma half-life for DA was 114.5 min in monkeys and 21.6 min in rats. Suzuki and Hierlihy (1993) investigated the excretion of DA in rats after intravenous dosing, and reported that DA was completely recovered in the urine within 160 min and that this excretion was not affected by treatment with probenecid, a competitive inhibitor of renal anion transport systems. The absorption rate of DA, estimated from the urinary excretion of DA after oral administration, was trace in both monkeys (4–7%) and rats (1.8%) (Truelove et al., 1996, 1997).

Ross et al. (2000) investigated the effects of DA on the uptake of glutamic acid in rat astrocytes, and reported that DA inhibited the uptake of glutamic acid in a dose-dependent manner. Some research groups reported that the uptake of glutamic acid across intestinal brush border membranes is predominantly mediated by a Na^+-dependent transport system (Rajendran et al., 1987; Nicklin et al., 1995; Mordrelle et al., 2000). These results led us to the hypothesis that DA absorption is mediated via the same transporter as that for glutamic acid. Furthermore, the possibility of DA absorption via monocarboxylic, dicarboxylic, or tricarboxylic acid transporter(s) as well as other transporters can be speculated.

In the present study, we investigated the absorption mechanism of DA using Caco-2 cells, which are morphologically and functionally similar to human small intestinal epithelial cells and widely used to predict intestinal "*in vivo*" absorption in humans (Hilgers et al., 1990).

2. Materials and methods

2.1. Materials

Dulbecco's modified Eagle's medium (DMEM), glycylsarcosine, benzoic acid, glutaric acid, acetic acid, succinic acid, citric acid, *p*-aminohippuric acid, tetraethylammonium, probenecid, L-proline, L-leucin, L-lysine, L-tryptophan were purchased from Wako Pure Chemical Industries, Ltd. (Osaka, Japan). L-Lactic acid, L-alanine, L-glutamic acid, L-asparatic acid, sulfobromophthalein, estron-3-sulfate, γ-aminobu-

* Corresponding author. Tel./fax: +81 0133 23 3902.
E-mail address: endotty@hoku-iryo-u.ac.jp (T. Endo).

0278-6915/$ - see front matter © 2011 Elsevier Ltd. All rights reserved.
doi:10.1016/j.fct.2011.06.001

tyric acid, 4,4′-diisothiocyanostilbene-2,2′-disulfonic acid (DIDS) were purchased from Sigma Chemical Co. (St. Louis, MO). Fetal bovine serum (FBS) and nonessential amino acid (NEAA) were obtained from Life Technologies (Rockville, MD). All other chemicals were commercial products of reagent grade.

Domoic acid (DA) was extracted with hot water from the red alga *Chondria armata* collected in July 2007 in Kagoshima Prefecture, Japan. The extract was purified by successive column chromatographies (3 × 45 and 2 × 45 cm) packed with reversed-phase silica gel (Wakosil 25 C18, Wako Pure Chemical Industries, Ltd., Osaka, Japan) and preparative HPLC with a Develosil ODS-5 column (1 × 25 cm, Nomura Chemical Co. Ltd., Seto, Japan). The mobile phase of 1% acetic acid in 10% acetonitrile was mainly used for purification. DA was monitored during the purification process by HPLC with UV detection (242 nm) according to a slightly modified version of Quilliam's method (Quilliam et al., 1989; Kotaki et al., 1999) in which a Develosil ODS-5 column (4.6 × 250 mm) with a mobile phase of 10% acetonitrile in 20 mM NaH_2PO_4 buffer (pH 2.5) was used. DA of 95% purity was obtained by above purification procedures. Absence of isomers such as isodomoic acids A and B and 5′-epi-domoic acid was also confirmed by HPLC analysis.

2.2. Cell culture

Caco-2 cells were obtained from RIKEN Cell Bank (Tsukuba, Japan) at passage 40, and used between passages 50 and 85. Caco-2 cells were cultured on permeable membranes (Cell Culture Insert, 0.4 μm, 0.9 cm^2 growth area; Becton Dickinson, Bedford, MA) in DMEM containing FBS (10%), NEAA (1%), streptomycin (100 μg/mL) and penicillin G (70 μg/mL) at 37 °C under a humidified atmosphere of 5% CO_2–95% air. The volume of culture medium on the apical and basolateral sides was 0.5 and 1.5 mL, respectively, and the medium was replaced every 2 or 3 days after seeding.

2.3. Transport experiments

Confluent cultures of Caco-2 cell monolayers (cultured for 21 or 22 days) with the transepithelial electrical resistances (TERs) of more than 350 Ω cm^2 were used for the transport experiments. These experiments were performed as described previously (Kimura et al., 2005, 2009). Briefly, the culture medium was replaced with the same volume of incubation medium, and the cell monolayers were preincubated at 37 °C or 4 °C for 20 min. The incubation medium used for the transport study was Hanks' balanced salt solution (137 mM NaCl, 5.36 mM KCl, 0.952 mM $CaCl_2$, 0.812 mM $MgSO_4$, 0.441 mM KH_2PO_4, 0.385 mM Na_2HPO_4) containing 25 mM D-glucose and 10 mM MES (pH 5.5, 6.0 or 6.5) or 10 mM HEPES (pH 7.0, 7.4 or 8.0). After preincubation, the cell monolayers were incubated with 100 μM DA in fresh incubation medium from either the apical or basolateral side for the indicated times at 37 °C or 4 °C.

In order to investigate the Na^+ dependence of the transcellular transport of DA, NaCl in the incubation medium was replaced with equimolar choline chloride or KCl, and Na_2HPO_4 was omitted from the medium. Furthermore, the cell monolayers were pretreated with 0.5 mM ouabain, a Na/K-ATPase inhibitor (Nicklin et al., 1995; Kimura et al., 1996), before incubation with DA. To examine the effect of an anion exchange inhibitor, the cell monolayers were coincubated at 37 °C for 60 min with 100 μM DA and 0.1 or 1.0 mM DIDS (Ogihara et al., 1999). To examine the effect of Cl^-, NaCl, KCl and $CaCl_2$ in the incubation medium were replaced with their respective gluconate salts. In the inhibition study, the cell monolayers were coincubated at 37 °C for 60 min with 100 μM DA and various compounds from the apical side.

2.4. Determination of domoic acid

DA was determined using an HPLC system consisting of a Shimadzu LC-10A pump and SPD-10A UV detector. The analytical conditions were as follows: column, Inertsil VP-ODS (4 × 250 mm; GL Sciences, Inc., Tokyo, Japan); mobile phase, 20 mM NaH_2PO_4 buffer (pH 2.5)/acetonitorile (90:10 (v/v)); flow rate, 0.8 mL/min; wavelength, 242 nm.

2.5. Statistical analyses

The data were analyzed by either Student's *t*-test or Scheffe's multiple comparison test after analysis of variance using the Statcell 12 program. The level of significance was set at $p < 0.05$.

3. Results

3.1. Time course of domoic acid transport across Caco-2 cell monolayers

The time course of the transcellular transport of DA across Caco-2 cell monolayers was investigated. Caco-2 cells were incubated at 37 °C with 100 μM DA from either the apical or basolateral side (Fig. 1). The transcellular transport of DA from the apical to basolateral side and from the basolateral to apical side increased linearly until 60 min. The apical-to-basolateral transport of DA was about twofold that in the opposite direction. As a result of the preferential transport of DA, further studies were focused on the apical-to-basolateral transport.

3.2. Effect of apical pH on the transcellular transport of domoic acid across Caco-2 cell monolayers

Caco-2 cell monolayers were incubated in incubation medium containing 100 μM DA on the apical side at 37 °C for 60 min at different pH values (Fig. 2). A change in pH from 7.4 to 6.4 did not affect the transcellular transport of DA, but DA transport at pH 5.5 (88.8%) and pH 8.0 (74.1%) was significantly lower than that at pH 7.4.

3.3. Effects of temperature and sodium on the transcellular transport of domoic acid across Caco-2 cell monolayers

The effects of low temperature and Na^+ on the transcellular transport of DA were examined (Fig. 3). Incubation at low temperature (4 °C) significantly reduced the transcellular transport of DA by 75.0%; however, Na^+-free conditions, achieved by the replacement of NaCl in incubation medium with equimolar choline chloride or KCl, did not decrease the transcellular transport of DA. In addition, pretreatment with 0.5 mM ouabain, a Na^+/K^+-ATPase inhibitor, did not decrease the transport of DA.

3.4. Effects of DIDS and chloride ions on the transcellular transport of domoic acid across Caco-2 cell monolayers

Transcellular transport of DA from the apical membrane via the anion exchanger was investigated (Fig. 4). Coincubation with DIDS, an anion exchange inhibitor, significantly inhibited the transcellular transport of DA in a dose-dependent manner: coincubation with 0.1 and 1.0 mM DIDS caused a 19.6 and 47.8% inhibition of DA transport, respectively.

The effect of Cl^- on the transcellular transport of DA was also examined (Fig. 5). The replacement of Cl^- by gluconate ions in the incubation medium on the apical side slightly but significantly decreased DA transport, and coincubation with DIDS caused a further decrease in DA transport. The replacement of Cl^- in the medium on both the apical and basolateral sides markedly decreased

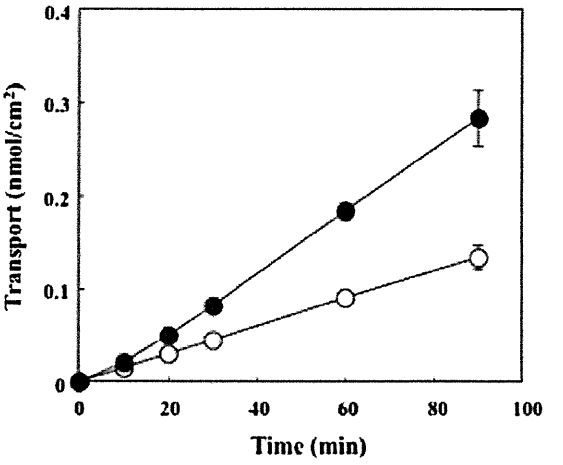

Fig. 1. Time course of domoic acid transport across Caco-2 cell monolayers. Caco-2 cell monolayers were incubated at 37 °C with 100 μM domoic acid added to the apical or basolateral medium. Each point represents the mean with S.E. for 3–6 determinations.

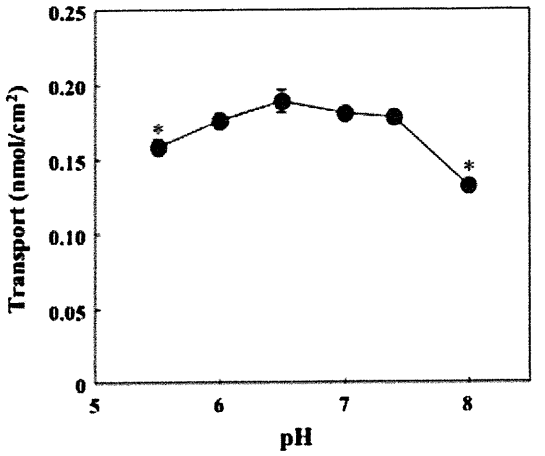

Fig. 2. Transcellular transport of domoic acid across Caco-2 cell monolayers at various pH values of the apical medium. Caco-2 cell monolayers were incubated at 37 °C for 60 min with 100 μM domoic acid added to the apical medium at various pH values. The pH of the basolateral medium was maintained at pH 7.4. Each point represents the mean with S.E. for five or six monolayers. *Significantly different from the apical medium at pH 7.4.

DA transport by 45.6%, and this decrease in DA transport was the same as that caused by coincubation with 1.0 mM DIDS (Fig. 4).

3.5. Effects of various compounds on the transcellular transport of domoic acid across Caco-2 cell monolayers

In order to characterize the transport system responsible for the apical-to-basolateral transport of DA, the effects of various compounds on DA transport were examined (Table 1). Coincubation with probenecid, a non-specific inhibitor of anion transport, significantly decreased the apical-to-basolateral transport of DA by 31.5%. In contrast, coincubation with tetraetylammonium, a typical substrate of organic cation transport systems (OCTs), and *p*-aminohippuric acid, a typical substrate of organic anion transport systems (OATs), did not decrease the transport of DA. Amino acids (L-leucin, L-proline, L-tryptophan, L-asparatic, L-glutamic and γ-aminobutyric acids), monocarboxylic acids (L-lactic, acetic and

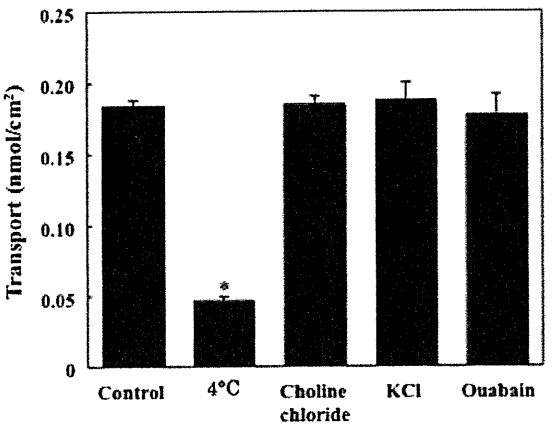

Fig. 3. Effects of temperature and sodium of transcellular transport of domoic acid across Caco-2 cell monolayers. Caco-2 cell monolayers were preincubated with 0.5 mM ouabain from both the apical and basolateral sides at 37 °C for 30 min. The cell monolayers were incubated with 100 μM domoic acid in HBSS, or sodium-trace HBSS (choline chloride and KCl) from the apical side at 4 or 37 °C for 60 min. Each point represents the mean with S.E. for five or six monolayers. *Significantly different from control.

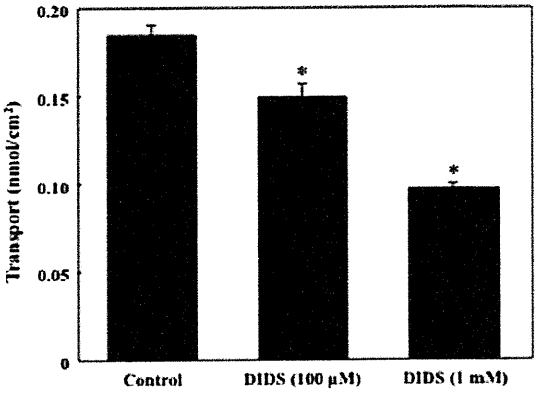

Fig. 4. Effect of DIDS on the transcellular transport of domoic acid across Caco-2 cell monolayers. Caco-2 cell monolayers were incubated at 37 °C for 60 min with 100 μM domoic acid added to the apical medium at pH 7.4 in the presence or absence of 0.1 or 1.0 mM DIDS. Each point represents the mean with S.E. for six monolayers. *Significantly different from the control.

benzoic acids), dicarboxylic acids (glutaric and succinic acids), tricarboxylic acid (citric acid), estrone-3-sulfate and sulfobromophthalein (substrates of the organic anion transporting polypeptide family; OATPs) and glycylsarcosine (a substrate of peptide transporters) did not decrease the apical-to-basolateral transport of DA (Table 1).

4. Discussion

We investigated the transcellular transport mechanism of DA using Caco-2 cell monolayers cultured on permeable membranes. The transcellular transport of DA from the apical to basolateral side was about twofold that in the opposite direction (Fig. 1). The transcellular transport of DA from the apical side was both temperature- and Cl^--dependent, and optimal at neutral pH, but was Na^+-independent (Figs. 2 and 3). In addition, the transport of DA from the apical to basolateral side was significantly decreased (approx. 50%) by coincubation with 1.0 mM DIDS (Fig. 4): the preferential direction of DA transport was diminished by the coincubation with

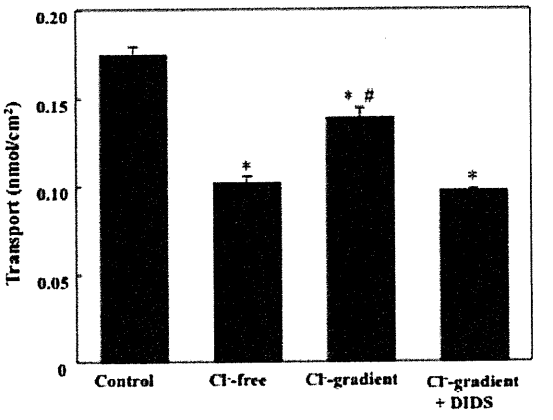

Fig. 5. Effect of chloride ion gradient on the transcellular transport of domoic acid across Caco-2 cell monolayers. Caco-2 cell monolayers were incubated at 37 °C for 60 min with 100 μM domoic acid added to the apical medium at pH 7.4 in the presence or absence of 1.0 mM DIDS. Cl^--free conditions: chloride ion-free apical and basolateral media, Cl^--gradient conditions: chloride ions-free apical medium. Each point represents the mean with S.E. for six monolayers. *Significantly different from the control. #Significantly different from the Cl^--free conditions or from the Cl^--gradient with DIDS.

Table 1
Effects of various compounds on the transcellular transport of domoic acid across Caco-2 cell monolayers.

Compound	Concentration (mM)	Domoic acid transport (% of control)
Control		100.0 ± 4.59
Tetraethylammonium	10	99.5 ± 3.54
p-Aminohippuric acid	10	97.8 ± 2.79
Probenecid	10	68.5 ± 2.76*
Succinic acid	10	97.3 ± 4.16
Glutaric acid	10	83.4 ± 2.82
Citric acid	10	87.6 ± 2.11
L-Lactic acid	10	88.1 ± 2.43
Acetic acid	10	89.9 ± 3.87
Benzoic acid	10	87.5 ± 5.07
Sulfobromophtalein	1	88.0 ± 4.25
Estrone-3-sulfate	1	90.3 ± 2.39
L-Asparatic acid	10	85.8 ± 3.75
L-Glutamic acid	10	85.7 ± 2.52
L-Alanine	10	84.6 ± 1.93
L-Proline	10	88.7 ± 4.87
L-Leucin	10	83.1 ± 3.92
L-Lysine	10	97.2 ± 2.76
L-Tryptophan	10	89.5 ± 4.56
γ-Aminobutyric acid	10	91.4 ± 3.86
Glycylsarcosine	10	93.6 ± 4.03

Caco-2 cell monolayers were coincubated with 100 μM domoic acid and various compounds on the apical side at 37 °C for 60 min. Each point represents the mean ± S.E. of 5–7 monolayers.
* Significantly different from the control.

DIDS. These results suggest that the transcellular transport of DA from the apical side is mediated by DIDS-sensitive anion transport systems. Anion exchangers (AEs) mediate the exchange of anions such as Cl^- and HCO_3^-. AEs are expressed in the intestine and Caco-2 cells (Alrefai et al., 2001; Jacob et al., 2002; Lecona et al., 2008), and inhibited by DIDS (Ogihara et al., 1999; Jacob et al., 2002). In the present study, the transport of DA was decreased by the replacement of Cl^- in the incubation media and the coincubation with DIDS (Fig. 5). These results imply that the transcellular transport of DA from the apical membrane is mediated by a DA/Cl^- antiporter, though further study using brush border membrane vesicles isolated from the small intestine is necessary to elucidate whether the intestinal absorption of DA is mediated by a DA/Cl^- antiporter.

DA is an amino acid with three carboxylic groups and one imino group in its structure, and structurally resembles glutamic acid, acting as a potent glutamate receptor agonist (Hampson et al., 1992; Lefebvre and Robertson, 2010). Glutamic acid uptake across intestinal brush border membranes purified from the human intestine and Caco-2 cells is mediated predominantly by a Na^+-dependent transport system (Rajendran et al., 1987; Nicklin et al., 1995; Mordrelle et al., 2000). However, the transcellular transport of DA across the apical membrane of Caco-2 cells was Na^+-independent (Fig. 3), and coincubation with 10 mM glutamic acid did not decrease DA transport, suggesting that DA does not share the same transporter as glutamic acid. On the other hand, Mordrelle et al. (1997) reported that the transport of glutamic acid in the rat intestinal crypt-like cell line IEC-17 was mediated not only by Na^+-dependent, but also by Na^+-independent transport systems, and coincubation with L-cystine, a substrate for Na^+-independent transport systems, significantly decreased the uptake of glutamate under Na^+-free conditions. In the present study, coincubation with L-cystine did not decrease the apical-to-basolateral transport of DA under Na^+-free conditions (data not shown), suggesting that the Na^+-independent transport system is not responsible for the intestinal absorption of DA. Although other amino acid transporters and dipeptide transporters are expressed in Caco-2 cells, similar to the intestine (Tsuji and Tamai, 1996; Hilgendorf et al., 2007), no significant inhibition of DA transport was observed by coincubation with neutral, basic or aromatic amino acids, or glycylsarcosine (a typical substrate of peptide transporters) (Table 1). These results suggest that the transcellular transport of DA across Caco-2 cells is not mediated by amino acid or peptide transporters.

OATPs are reported to be expressed in and localized at the brush border membrane of both the human small intestine and Caco-2 cells, where they mediate the transport of estrone-3-sulfate and sulfobromophtalein under acidic conditions (Sai et al., 2006). In the present study, coincubation with estrone-3-sulfate or sulfobromophtalein did not decrease DA transport (Table 1), and the transport of DA from apical side was lower under acidic conditions (Fig. 2). OATPs appear not to be involved in the transcellular transport of DA from the apical side in Caco-2 cells.

Uptake of citrate (a tricarboxylate) from the apical membrane of Caco-2 cells is reported to be mediated by transporters, and uptake of dicarboxylic compounds, such as succinic and glutaric acid, is also reported to be mediated by dicarboxylic transporters (Weerachayaphorn and Pajor, 2008). However, coincubation with citric acid, succinic acid or glutaric acid did not affect DA transport (Table 1). Thus, DA transport may not share the same transporter as tricarboxylic or dicarboxylic acids.

It has been reported that various monocarboxylic acid transport family (MCTs) isoforms (MCT1 and MCT3–MCT6) are expressed in Caco-2 cells, of which H^+-linked MCT1 is the most abundant (Hadjiagapiou et al., 2000). However, the optimal pH of the transport of DA from the apical side occurred under neutral conditions (Fig. 2), and was not inhibited by the presence of monocarboxylic acids (Table 1), suggesting that MCTs are not responsible for the transcellular transport of DA.

We previously reported that the uptake of 4-chloro-2-methylphenoxyacetic acid (MCPA) in Caco-2 cells is mediated via MCTs (Kimura et al., 2008, 2009), of which the absorption rate was reported to be notably high (Lappin et al., 2002). The apical-to-basolateral transport of MCPA (50 μM) at 60 min and pH 6.0 under the same conditions of the present experiment was about 5.9 nmol/cm^2 (our unpublished data). In contrast, the transport of DA (100 μM) at 60 min and pH 7.4 was markedly lower (about 0.18 nmol/cm^2, Fig. 1), and the absorption rate of DA was reported to be trace (Truelove et al., 1996, 1997). Thus the contribution of DIDS-sensitive transport in "*in vivo* absorption of DA" may be small.

Coincubation with tetraethylammonium (a typical substrate of OCTs) or *p*-aminohippuric acid (a typical substrate of OATs) did not decrease the transport of DA, although DA is a zwitterion at a physiological pH.

In conclusion, we elucidated the contribution of DIDS-sensitive transport in DA transport in Caco-2 cells, although the absorption rates of DA in experimental animals were reported to be trace (Truelove et al., 1996, 1997). Against expectations, DA transport appears not to share a transport system with glutamic acid.

Conflict of Interest

The authors declare that there are no conflicts of interest.

Acknowledgments

This work was supported by Grants-in-Aid from Japan Society for the Promotion of Science (C21590135) and International Fund for Animal Welfare (IFAW).

References

Alrefai, W.A., Tyagi, S., Nazir, T.M., Barakat, J., Anwar, S.S., Hadjiagapiou, C., Bavishi, D., Sahi, J., Malik, P., Goldstein, J., Layden, T.J., Ramaswamy, K., Dudeja, P.K., 2001. Human intestinal anion exchanger isoforms: expressio, distribution, and membrane localization. Biochim. Biophys. Acta 1511, 17–27.

Hadjiagapiou, C., Schmidt, L., Dudeja, P.K., Layden, T.J., Ramaswamy, K., 2000. Mechanism(s) of butyrate transport in Caco-2 cells: role of monocarboxylate transporter 1. Am. J. Physiol. Gastrointest. Liver Physiol. 279, G775–G780.

Hampson, D.R., Huang, X.P., Wells, J.W., Walter, J.A., Wright, J.L., 1992. Interaction of domoic acid and several derivatives with kainic acid and AMPA binding sites in rat brain. Eur. J. Pharmacol. 218, 1–8.

Hilgendorf, C., Ahlin, G., Seithel, A., Artursson, P., Ungell, A.L., Karlsson, J., 2007. Expression of thirty-six drug transporter genes in human intestine, liver, kidney, and organotypic cell lines. Drug Metab. Dispos. 35, 1333–1340.

Hilgers, A.R., Conradi, R.A., Burton, P.S., 1990. Caco-2 cell monolayers as a model for drug transport across the intestinal mucosa. Pharm. Res. 7, 902–910.

Jacob, P., Rossmann, H., Lamprecht, G., Kretz, A., Neff, C., Lin-Wu, E., Gregor, M., Groneberg, D.A., Kere, J., Seidler, U., 2002. Down-regulated in adenoma mediates apical Cl^-/HCO^{3-} exchange in rabbit, rat, and human duodenum. Gastroenterology 122, 709–724.

Kimura, O., Endo, T., Sakata, M., 1996. Comparison of cadmiun uptakes from apical and basolateral membranes of LLC-PK_1 cells. Toxicol. Appl. Pharmacol. 137, 301–306.

Kimura, O., Endo, T., Hotta, Y., Sakata, M., 2005. Effects of P-glycoprotein inhibitors on transepithelial transport of cadmium in cultured renal epithelial cells, LLC-PK_1 and LLC-GA5-COL 150. Toxicology 208, 123–132.

Kimura, O., Tsukagoshi, K., Endo, T., 2008. Uptake of 4-chloro-2-methylphenoxyacetic acid (MCPA) from the apical membrane of Caco-2 cells by the monocarboxylic acid transporter. Toxicol. Appl. Pharmacol. 227, 325–330.

Kimura, O., Tsukagoshi, K., Endo, T., 2009. Uptake of phenoxyacetic acid derivatives into Caco-2 cells by the monocarboxylic acid transporters. Toxicol. Lett. 189, 102–109.

Kotaki, Y., Koike, K., Sato, S., Ogata, T., Fukuyo, Y., Kodama, M., 1999. Confirmation of domoic acid production of *Pseudo-nitzschia multiseries* isolated from Ofunato Bay, Japan. Toxicon 37, 677–682.

Lappin, G.J., Hardwick, T.D., Stow, R., Pigott, G.H., van Ravenzwaay, B., 2002. Absorption, metabolism and excretion of 4-chloro-2-methylphenoxyacetic acid (MCPA) in rat and dog. Xenobiotica 32, 153–163.

Lecona, E., Olmo, N., Turnay, J., Santiago-Gómez, A., López de Silanes, I., Gorospe, M., Lizarbe, M.A., 2008. Kinetic analysis of butyrate transport in human colon adenocarcinoma cells reveals two different carrier-mediated mechanisms. Biochem. J. 409, 311–320.

Lefebvre, K.A., Robertson, A., 2010. Domoic acid and human exposure risks: a review. Toxicon 56, 218–230.

Mordrelle, A., Huneau, J.F., Tomé, D., 1997. Sodium-dependent and -independent transport of L-glutamate in the rat intestinal crypt-like cell line IEC-17. Biochem. Biophys. Res. Commun. 233, 244–247.

Mordrelle, A., Jullian, E., Costa, C., Cormet-Boyaka, E., Benamouzig, R., Tomé, D., Huneau, J.F., 2000. EAAT1 is involved in transport of L-glutamate during differentiation of the Caco-2 cell line. Am. J. Physiol. Gastrointest. Liver Physiol. 279, G366–G373.

Nicklin, P.L., Irwin, W.J., Hassan, I.F., Mackay, M., Dixon, H.B.F., 1995. The transport of acidic amino acids and their analogues across monolayers of human intestinal absorptive (Caco-2) cells in vitro. Biochim. Biophys. Acta 1269, 176–186.

Ogihara, T., Tamai, I., Tsuji, A., 1999. Structural characterization of substrates for the anion exchange transporter in Caco-2 cells. J. Pharm. Sci. 88, 1217–1221.

Quilliam, M.A., Sim, P.G., McCulloch, A.W., McInnes, A.G., 1989. High-performance liquid chromatography of domoic acid, a marine neurotoxin, with application to shellfish and plankton. Int. J. Environ. Anal. Chem. 36, 139–154.

Rajendran, V.M., Harig, J.M., Adams, M.B., Ramaswamy, K., 1987. Transport of acidic amino acids by human jejunal brush-border membrane vesicles. Am. J. Physiol. 252, G33–G39.

Ross, I.A., Johnson, W., Sapienza, P.P., Kim, C.S., 2000. Effects of the seafood toxin domoic acid on glutamate uptake by rat astrocytes. Food Chem. Toxicol. 38, 1005–1011.

Sai, Y., Kaneko, Y., Ito, S., Mitsuoka, K., Kato, Y., Tamai, I., Artursson, P., Tsuji, A., 2006. Predominant contribution of organic anion transporting polypeptide OATP-B (OATP2B1) to apical uptake of estrone-3-sulfate by human intestinal Caco-2 cells. Drug Metab. Dispos. 34, 1423–1431.

Suzuki, C.A.M., Hierlihy, S.L., 1993. Renal clearance of domoic acid in the rat. Food Chem. Toxicol. 31, 701–706.

Truelove, J., Iverson, F., 1994. Serum domoic acid clearance and clinical observations in the cynomolgus monkey and Sprague-Dawley rat following a single i.v. dose. Bull. Environ. Contam. Toxicol. 52, 479–486.

Truelove, J., Mueller, R., Pulido, O., Iverson, F., 1996. Subchronic toxicity study of domoic acid in the rat. Food Chem. Toxicol. 34, 525–529.

Truelove, J., Mueller, R., Pulido, O., Martin, L., Fernie, S., Iverson, F., 1997. 30-day oral toxicity study of domoic acid in cynomolgus monkeys: lack of overt toxicity at doses approaching the acute toxic dose. Nat. Toxins 5, 111–114.

Tsuji, A., Tamai, I., 1996. Carrier-mediated intestinal of drugs. Pharm. Res. 13, 963–977.

Weerachayaphorn, J., Pajor, A.M., 2008. Identification of transport pathways for citric acid cycle intermediates in the human colon carcinoma cell line, Caco-2. Biochim. Biophys. Acta 1778, 1051–1059.

Wright, J.L.C., Boyd, R.K., de Freitas, A.S.W., Falk, M., Foxall, R.A., Jamieson, W.D., Laycock, M.V., McCulloch, A.W., McInnes, A.G., Odense, P., Pathak, V.P., Quilliam, M.A., Ragan, M.A., Sim, P.G., Thibault, P., Walter, J.A., Gilgan, M., Richard, D.J.A., Dewar, D., 1989. Identification of domoic acid, a neuroexcitatory amino acid, in toxic mussels from eastern Prince Edward Island. Can. J. Chem. 67, 481–490.

SOLA, 2011, Vol. 7A, 005−008, doi:10.2151/sola.7A-002

Solubility of Iron in the Aerosol Collected during Kosa (Asian Dust) Events in Japan

Ikuko Mori[1], Masataka Nishikawa[1], Atsushi Shimizu[1], Masamitsu Hayasaki[2], and Takumi Takasuga[3]
[1]*National Institute for Environmental Studies, Tsukuba, Japan*
[2]*Center for Environmental Remote Sensing, Chiba University, Chiba, Japan*
[3]*Shimadzu Techno-Research, Kyoto, Japan*

Abstract

The main contributor of aerosol particulate soluble iron to Japan and the Pacific Ocean has been investigated using data obtained during the research campaign entitled "A Study on Dust and Sand Storms" conducted by the Ministry of the Environment, Japan. The concentration of particulate soluble iron was not correlated to total iron concentration. Particulate iron solubility ranged from less than 1% to 6%. It was low when the air mass was dominated by kosa aerosols, and high when the air mass was dominated by pollutants. Durations for the kosa and pollution events over Jeju Island, Matsue, and the Pacific Ocean in April and May 2007 were estimated using a Chemical Weather Forecasting System (CFORS). The estimated durations of the pollution events at Jeju and Matsue were slightly shorter than those of the kosa events. The calculated duration of the pollution event over the Pacific Ocean was only three hours, much shorter than that of the kosa event. Kosa aerosols are the main contributor of soluble iron to the Pacific Ocean; however anthropogenic aerosols should not be discounted as contributors of soluble iron to an area off the coast of the Asian continent.

1. Introduction

Iron is essential for the growth of organisms and may limit phytoplankton primary production, especially in the remote ocean, and several studies on the solubility of atmospheric particulate iron have been conducted (Zhuang et al. 1992; Spokes et al. 1994; Fan et al. 2006). Previous studies considered the solubility of aerosol iron mainly from two aspects; differences in leaching processes and differences in the source of the iron. Laboratory studies suggested that iron solubility should be predictable in terms of the pH/solubility relationship (Spokes et al. 1994) and demonstrated that acidification by gaseous nitric acid led to an increase in water-soluble iron (Duvall et al. 2008). Meskhidze et al. (2003) predicted that the pH estimated by using the observed nitrate ion and gaseous nitric acid concentrations was low enough to facilitate iron mobilisation in mineral dust from East Asia. On the other hand, the laboratory study conducted by Schroth et al. (2009) showed that the solubility of iron in an aerosol could vary depending on its source; the measured solubility of iron in arid soils was less than 1%, that in glacially produced soils was 2–3%, whereas in oil combustion products it was 77–81%. Acid processing of insoluble iron was not significant in authentic aerosol samples (Chuang et al. 2005; Baker et al. 2006). Aguilar-Islas et al. (2010) concluded, based on the result of leaching experiments and using data from the literature, that more variability in aerosol iron solubility resulted from differences in aerosol type than from different leaching protocols.

The main contributing source of soluble iron, especially to the remote ocean, is still a matter of controversy. Chuang et al. (2005) concluded, based on the results of chemical analysis, that the iron released by fuel combustion was the main contributor of the soluble iron in aerosols collected in Jeju, Korea. Sedwick et al. (2007) agreed with this conclusion following chemical analysis of aerosols collected from the Sargasso Sea. A model calculation suggested that anthropogenic emissions contributed approximately 70% and 85% of the annual dry deposition of soluble iron to the surface ocean near Bermuda and Ireland, respectively (Sholkovitz et al. 2009). Another model calculation suggested that iron from combustion processes can represent up to 50% of the total iron deposited, but over open ocean regions it usually contributes less than 5% of the total iron, with the highest values (< 30%) close to the East Asian continent in the North Pacific (Luo et al. 2008).

In this paper, the main contributor of soluble iron to Japan and the Pacific Ocean was investgated using data obtained during the research initiative entitled "A study on Dust and Sand Storms" conducted by the Ministry of the Environment, Japan.

2. Aerosol samples and methods

Since 2002 the Ministry of the Environment of Japan has conducted a research campaign entitled "A Study on Dust and Sand Storms" to investigate the physical and chemical characteristics of kosa (Asian dust) aerosols. During this research, total suspended particulates (TSP) were collected in nine locations throughout Japan (Fig. 1) using high volume samplers with quartz fibre filters, when kosa events were observed in China.This aerosol sampling has been conducted a few times each year. The aerosol mass concentration and the concentrations of the chemical components of the aerosols were determined by the procedure described by Mori et al. (2002). In brief, water-soluble components were extracted using ultrapure water, and bulk components were digested using a mixture of nitric, perchloric, and hydrofluoric acids. Aerosol vertical distribution was measured by lidar (Shimizu et al. 2004). The concentrations of suspended particulate matter (SPM) and sulfur dioxide (SO_2) were measured simultaneously. Five events (Table 1) were selected for discussion of the characteristics of water soluble iron in aerosols collected during heavy dust events. Results of backward trajectory analyses revealed that the air masses came to Japan from the Asian continent during these events. Details of the research campaign and the selected heavy dust events are described in MOE (2009).

3. Results and discussion

3.1 Total and water soluble iron concentrations

Concentrations of TSP, total iron (Fe), and water soluble iron in the aerosols collected during five heavy dust events over Japan were in the ranges 66–509 μg m^{-3}, 1.7–20.2 μg m^{-3}, < 0.01–0.13 μg m^{-3}, respectively. The concentration of total iron increased with an increase in the TSP concentration. However, the concentration of water soluble iron did not increase with increases in TSP or total iron concentrations (Fig. 2). This result agreed with that from aerosol monitoring in Jeju Island, Korea (Chuang et al. 2005). The particulate soluble iron concentration is not correlated to the total iron concentration in the Asian outflow atmosphere.

Corresponding author: Ikuko Mori, National Institute for Environmental Study, 16-2 Onogawa, Tsukuba 305-8506, Japan. E-mail: mori.ikuko@nies.go.jp.

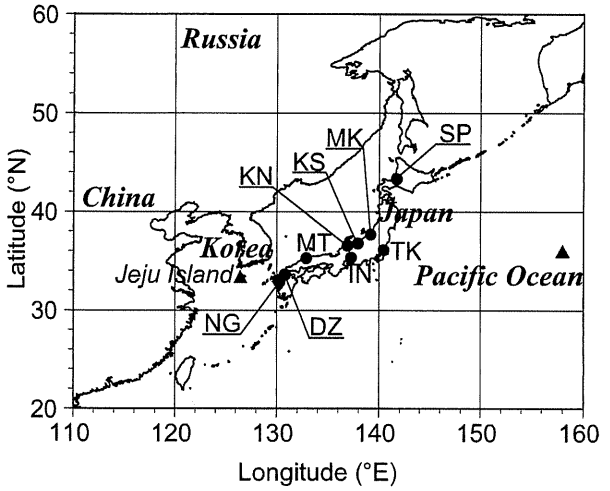

Fig. 1. TSP sampling locations (circles). DZ: Dazaifu, IN: Inuyama, KN: Kanazawa, KS: Kosugi, MK: Maki, MT: Matsue, NG: Nagasaki, SP: Sapporo, TK: Tsukuba. Locations selected for the CFORS calculation (Jeju Island and the Pacific Ocean) are also shown (triangles).

Table 1. Selected heavy dust event.

Event	Date	Note
1	8–9 April 2006	Kosa
2	18–19 April 2006	Kosa
3	1–2 April 2007	Kosa (TAD-2007*)
4	8–9 May 2007	Pollution**
5	26–27 May 2007	Kosa

*: Typical Asian Dust 2007
**: Hayasaki et al. (2008) and Ohara et al. (2008)

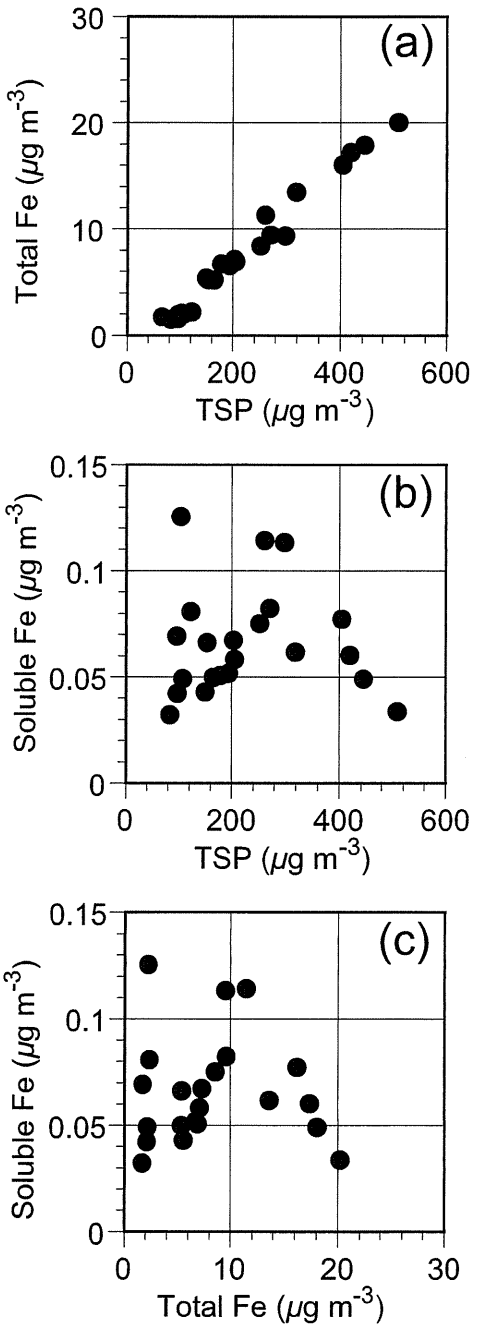

Fig. 2. The relationship between (a) particulate total Fe and TSP (b) particulate soluble Fe and TSP, and (c) particulate soluble Fe and total Fe concentration for the aerosols collected during heavy dust events in Japan.

3.2 Particulate iron solubility and source

The particulate iron solubility ranged from less than 1% to 6% during the five heavy dust events in Japan. This result is consistent with that reported for the Jeju aerosol (Chuang et al. 2005; Duvall et al. 2008) and with that for the aerosol collected over the Sagrasso Sea (Sedwick et al. 2007).

Laboratory studies demonstrated that the solubility of iron in loess was less than 1% (Duvall et al. 2008; Schroth et al. 2009). In contrast, the solubility of iron in oil combustion products ranged from 49–100% (Henry and Knapp 1980; Schroth et al. 2009). These results derived from laboratory studies indicated that particulate iron solubility in aerosols could be controlled by the source of the aerosol.

To investigate the relationship between the solubility of particulate iron and the contribution of kosa to the aerosol, the particulate iron solubility was plotted against the ratio of the aluminium concentration to TSP (Fig. 3), which shows the particulate iron solubility decreased as the Al/TSP increased. Aluminium is often used as an indicator of mineral aerosols (Uematsu et al. 1983; Duce 1995), and therefore the higher the Al/TSP, the higher the contribution of kosa to the aerosol. That kosa was the main contributor to the aerosol was also supported by the observation that its Fe/Al value approached 0.5, very close to the Fe/Al value for Simulated Asian Mineral Dust certified reference material (0.51) (Nishikawa et al. 2000), as Al/TSP increased (Fig. 4). From these results, it could be concluded that the solubility of particulate iron was ca 1% when kosa aerosol was the predominant material in the atmosphere.

The particulate iron solubility was also plotted against the ratio of the sum of the concentrations nitrate (NO_3^-) and non-sea salt sulfate ($nssSO_4^{2-}$) ions (Anion) to TSP (Fig. 5) in order to investigate the relationship between iron solubility and the contribution of anthropogenic aerosol. Sulfate and nitrate ions are mainly formed from substances supplied to the atmosphere through human activity. Generally, a higher Anion/TSP value indicates a higher contribution of an anthropogenic aerosol. Figure 5 shows that the particulate iron solubility was high when the Anion/TSP was high. This result suggested that particulate iron solubility is high when anthropogenic aerosols are predominant in the atmosphere.

The dependency of particulate iron solubility on air mass type was also investigated. The air mass was categorised: 1) kosa, 2) kosa + pollutant, 3) pollutant; according to the analytical results of lidar measurements and SPM and SO_2 measurements (MOE

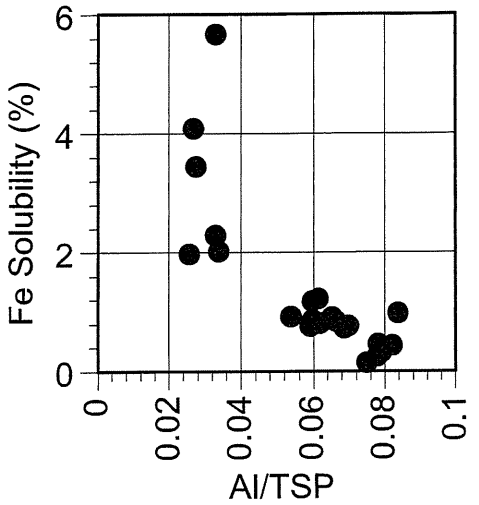

Fig. 3. The relationship between particulate iron solubility and Al/TSP for the aerosols collected during heavy dust events in Japan.

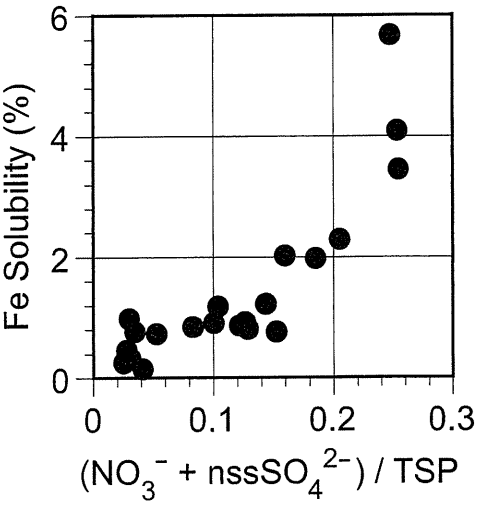

Fig. 5. The relationship between particulate iron solubility and (NO_3^- + $nssSO_4^{2-}$)/TSP for the aerosols collected during heavy dust events in Japan.

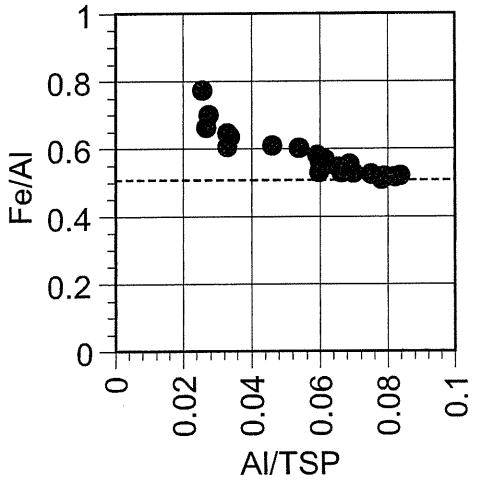

Fig. 4. The relationship between Fe/Al and Al/TSP for the aerosols collected during heavy dust events in Japan. The dotted line represents Fe/Al for Simulated Asian Mineral Dust certified reference material (CJ-2).

2009). The solubility of iron in the aerosol collected when the air mass was categorised as kosa was low, and the iron solubility when the air mass was categorised as pollutant was high (Table 2).

These results were consistent with the results of the laboratory study as described above. Particulate iron solubility in the atmosphere over Japan would be controlled by the aerosol source as described by Schroth et al. (2009) and Aguilar-Islas et al. (2010).

3.3 Primary contributor of particulate soluble iron to Japan and the Pacific Ocean

The soluble iron concentrations in the aerosols in each air mass category are summarised in Table 2. Differences in the soluble iron concentration in each air mass category were insignificant, although the differences in the iron solubility were significant. Therefore, iron solubility was not a key factor in controlling the amount of particulate soluble iron. The duration of each event (kosa, pollution or a combination of the two) would be the key factor in controlling the quantity of particulate soluble iron.

To estimate the duration of a kosa event and a pollution event, dust and sulfate concentrations throughout April and May 2007 were calculated using a chemical weather forecasting system (CFORS) (Uno et al. 2004). Three locations: 1) Jeju, Korea, 2) Matsue, Japan, 3) the Pacific Ocean (Fig. 1); were selected for this analysis. In this paper, when the calculated dust concentration near the surface exceeded 100 μg m^{-3} was categorised as the kosa event, and when the calculated sulfate concentration near the surface exceeded 10 μg m^{-3} was categorised as the pollution event. These threshold values were determined based upon CFORS results during kosa and pollution events observed in Matsue. The calculated total duration of the kosa event at Jeju and Matsue was slightly longer than that for the pollution event (Table 3). This suggested that a kosa event supplies more soluble iron to these locations than does a pollution event. This result contradicts that of Chuang et al. (2005) who concluded that soluble iron was mainly derived from anthropogenic activity with mineral dust making a negligible contribution. However, the calculated total duration of the pollution event over the Pacific Ocean was only three hours, and was much shorter than the kosa event (Table 3). This suggested that kosa aerosol is the main contributor of particulate soluble iron to the Pacific Ocean. This finding is consistent with that of Sholkovitz et al. (2009) that the annual mean dry deposition of

Table 2. Median and range (in parentheses) of TSP, particulate total iron, particulate soluble iron, and iron solubility for the aerosols collected during high TSP events in Japan. Air mass was categorised according to the results of lidar, SPM and SO_2 measurements.

Air mass	TSP (μg m^{-3})	Total Fe (μg m^{-3})	Soluble Fe (μg m^{-3})	Fe Solubility (%)
Kosa	404 (149–509)	16.2 (5.5–20.2)	0.061 (0.034–0.115)	0.46 (0.17–1.00)
Kosa + Pollutant	198 (66–298)	7.0 (1.9– 9.6)	0.063 (< 0.01–0.114)	0.88 (< 0.1–1.24)
Pollutant	100 (83–122)	2.1 (1.7– 2.4)	0.060 (0.033–0.126)	2.9 (2.0– 5.7)

Table 3. Estimated duration of the kosa and pollution events over Jeju Island, Matsue, and the Pacific Ocean by CFORS in April and May 2007.

(h)	Kosa	Pollution
Jeju Island, Korea	312	165
Matsue, Japan	315	255
Pacific Ocean	72	3

soluble iron at Barbados and Izana is dominated by soil dust, even though the study location was different. It is also consistent with the conclusions based on the Saharan dust study by Baker et al. (2006). We conclude that kosa aerosols are the main contributor of soluble iron to remote ocean, such as those of the Pacific Ocean, but that anthropogenic aerosols should not be discounted as sources of soluble iron area of sea off the coast of the Asian continent.

4. Summary

The following conclusions were derived from the results of the research campaign entitled "A Study on Dust and Sand Storms" conducted by the Ministry of the Environment, Japan:

1. The particulate soluble iron concentration in the Asian outflow atmosphere is not correlated to the total iron concentration.
2. The solubility of particulate iron in the atmosphere over Japan depends upon the source of the aerosol.
3. Kosa aerosols are the main contributor of soluble iron to the remote ocean, such as the Pacific Ocean, but anthropogenic aerosols should not be discounted as a source of soluble iron to areas off the coast of the Asian continent.

Acknowledgements

The authors thank the members of "A Study on Dust and Sand Storms" for collecting the aerosol samples and for various datasets. Part of this research was supported by the Environment Research and Technology Development Fund (B-0901) of the Ministry of the Environment, Japan. This paper contributes to research undertaken under the TEMM-WG1.

References

Aguilar-Islas, A. M., J. Wu, R. Rember, A. M. Johansen, and L. M. Shank, 2010: Dissolution of aerosol-derived iron in seawater: Leach solution chemistry, aerosol type, and colloidal iron fraction. *Marine Chem.*, **120**, 25–33.

Baker, A. R., T. D. Jickells, M. Witt, and K. L. Linge, 2006: Trends in the solubility of iron, aluminium, manganese and phosphorus in aerosol collected over the Atlantic Ocean. *Marine Chem.*, **98**, 43–58.

Chuang, P. Y., R. M. Duvall, M. M. Shafer, and J. J. Schauer, 2005: The origin of water soluble particulate iron in the Asian atmospheric outflow. *Geophys. Res. Lett.*, **32**, L07813, doi:10.129/2004GL021946.

Duce, R. A., 1995: Sources, distributions, and fluxes of mineral aerosols and their relationship to climate: in Aerosol Forcing of Climate, Wiley, 43–72 pp.

Duvall, R. M., B. J. Majestic, M. M. Shafer, P. Y. Chuang, B. R. T. Simoneit, and J. J. Schauer, 2008: The water-soluble fraction of carbon, sulfur, and crustal elements in Asian aerosols and Asian soils. *Atmos. Environ.*, **42**, 5872–5884.

Fan, S.-M., W. J. Moxim, and H. L. II, 2006: Aeolian input of bioavailable iron to the ocean. *Geophys. Res. Lett.*, **33**, L070602, doi:10.1029/2005GL024852.

Hayasaki, M., T. Ohara, J. Kurokawa, I. Uno, and A. Shimizu, 2008: Episodic pollution of photochemical ozone during 8-9 May 2007 over Japan: Observational data analyses. *J. Japan Soc. Atmos. Environ.*, **43**, 225–237.

Henry, W. M., and K. T. Knapp, 1980: Compound forms of fossil fuel fly ash emissions. *Environ. Sci. Technol.*, **14**, 450–456.

Luo, C., N. Mahowald, T. Bond, P. Y. Chuang, P. Artaxo, R. Siefert, Y. Chen, and J. Schauer, 2008: Combustion iron distribution and deposition. *Global Biogeochem. Cycles*, **22**, GB1012, doi:10.1029/2007GB002964.

Meskhidze, N., W. L. Chameides, A. Nenes, and G. Chen, 2003: iron mobilization in mineral dust: Can anthropogenic SO_2 emissions affect ocean productivity?. *Geophys. Res. Lett.*, **30**, 2085.

MOE, 2009: Ministry of the Environment, Japan Kosa jittai kaimei chosa hokokusyo, 169 pp.

Mori, I., M. Nishikawa, H. Quan, and M. Morita, 2002: Estimation of the concentration and chemical composition of kosa aerosols at their origin. *Atmos. Environ.*, **36**, 4569–4575.

Nishikawa, M., Q. Hao, and M. Morita, 2000: 0363 Preparation and evaluation of certified reference materials for Asian mineral dust. *Global Environ. Res.*, **4**, 103–113.

Ohara, T., I. Uno, J.-I. Kurokawa, M. Hayasaki, and A. Shimizu, 2008: Episodic pollution of photochemical ozone during 8–9 May 2007 over Japan –Overview–. *J. Japan Soc. Atmos. Environ.*, **43**, 198–208.

Schroth, A. W., J. Crusius, E. R. Sholkovitz, and B. C. Bostick, 2009: Iron solubility driven by speciation in dust sources to the ocean. *Nat. Geosci.*, **2**, 337–340.

Sedwick, P. N., E. R. Sholkovitz, and T. M. Church, 2007: Impact of anthropogenic combustion emissions on the fractional solubility of aerosol iron: Evidence from the Sargasso Sea. *Geochem. Geophys. Geosys.*, **8**, Q10Q06, doi:10.1029/2007GC001586.

Shimizu, A., N. Sugimoto, I. Matsui, K. Arao, I. Uno, T. Murayama, N. Kagawa, K. Aoki, A. Uchiyama, and A. Yamazaki, 2004: Continuous observations of Asian dust and other aeroosols by polarization lidars in China and Japan during ACE-Asia. *J. Geophys. Res.*, **109**, D19S17, doi:10.1029/2002JD003253.

Sholkovitz, E. R., P. N. Sedwick, and T. M. Church, 2009: Influence of anthropogenic combustion emissions on the deposition of soluble aerosol iron to the ocean: Empirical estimates for island sites in the North Atlantic. *Geochim. Cosmochim. Acta*, **73**, 3981–4003.

Spokes, L. J., T. D. Jickells, and B. Lim, 1994: Solubilisation of aerosol trace metals by cloud processing: A laboratory study. *Geochim. Cosmochim. Acta*, **58**, 3281–3287.

Uematsu, M., R. A. Duce, J. M. Prospero, L. Chen, J. T. Merrill, and R. L. McDonald, 1983: Transport of mineral aerosol from Asia over the North Pacific Ocean. *J. Geophys. Res.*, **88**, 5343–5352.

Uno, I., S. Satake, G. R. Carmichael, Y. Tang, Z. Wang, T. Takemura, N. Sugimoto, A. Shimizu, T. Murayama, T. A. Cahill, S. Cliff, M. Uematsu, S. Ohta, P. K. Quinn, and T. S. Bates, 2004: Numerical study of Asian dust transport during the springtime of 2001 simulated with the Chemical Weather Forcasting System (CFORS) model. *J. Geophys. Res.*, **109**, D19S24, doi:10.1029/2003JD004222, 2004.09.

Zhuang, G., Z. Yi, R. A. Duce, and P. R. Brown, 1992: Link between iron and sulphur cycles suggested by detection of Fe (II) in remote marine aerosols. *Nature*, **355**, 537–539.

Manuscript received 3 November 2010, accepted 22 December 2010
SOLA: http://www.jstage.jst.go.jp/browse/sola/